Article

Developmental Cell

Distinct p53 isoforms code for opposing transcriptional outcomes

Graphical abstract

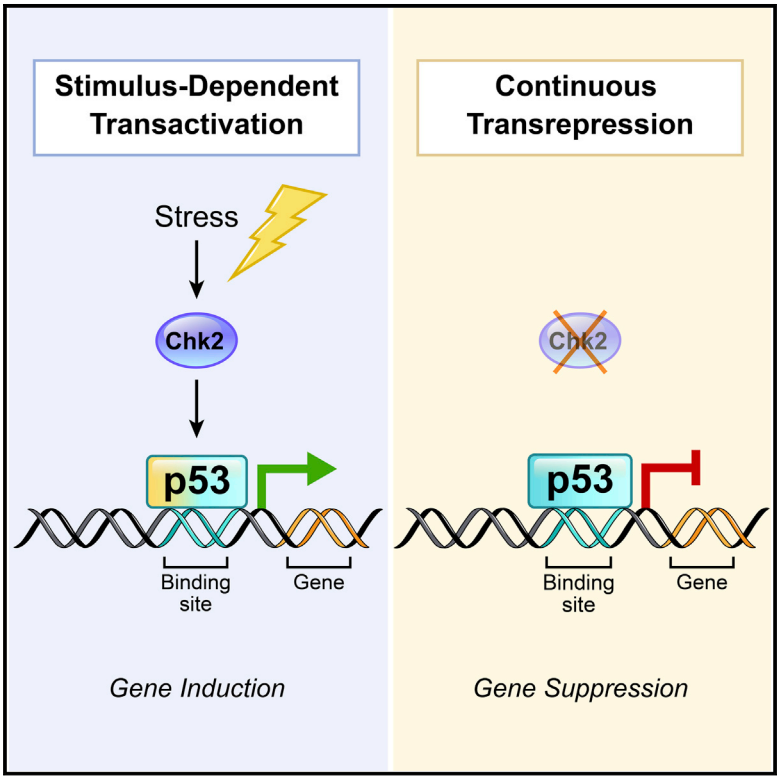

Authors

Annika Wylie, Amanda E. Jones, Simanti Das, Wan-Jin Lu, John M. Abrams

Correspondence

john.abrams@utsouthwestern.edu

In brief

Wylie et al. find that p53 mediates continuous repression in unstressed cells through canonical DNA binding sites that confer stimulus-dependent transactivation at earlier developmental stages. They further show that distinct p53 isoforms mediate these opposing transcriptional outcomes. The results expand p53 modalities and have important implications for understanding tumor suppression by p53.

Highlights

- Transcriptional repression by p53 is a constitutive "ground-state" function
- p53 transactivation and transrepression are genetically distinct
- p53 repression operates through direct occupancy of canonical DNA binding sites
- Opposing transcriptional outputs assign to distinct p53 isoforms and residues

Wylie et al., 2022, Developmental Cell *57*, 1833–1846
August 8, 2022
https://doi.org/10.1016/j.devcel.2022.06.015

CellPress

Developmental Cell

CellPress

Article

Distinct p53 isoforms code for opposing transcriptional outcomes

Annika Wylie,[1] Amanda E. Jones,[1] Simanti Das,[1] Wan-Jin Lu,[2] and John M. Abrams[1,3,*]
[1]Department of Cell Biology, University of Texas Southwestern Medical Center, Dallas, TX 75390, USA
[2]Institute for Stem Cell Biology and Regenerative Medicine, Stanford University School of Medicine, Stanford, CA 94305, USA
[3]Lead contact
*Correspondence: john.abrams@utsouthwestern.edu
https://doi.org/10.1016/j.devcel.2022.06.015

SUMMARY

p53 genes are conserved transcriptional activators that respond to stress. These proteins can also downregulate genes, but the mechanisms are not understood and are generally assumed to be indirect. Here, we investigate synthetic and native *cis*-regulatory elements in *Drosophila* to examine opposing features of p53-mediated transcriptional control *in vivo*. We show that transcriptional repression by p53 operates continuously through canonical DNA binding sites that confer p53-dependent transactivation at earlier developmental stages. p53 transrepression is correlated with local H3K9me3 chromatin marks and occurs without the need for stress or Chk2. In sufficiency tests, two p53 isoforms qualify as transrepressors and a third qualifies as a transcriptional activator. Targeted isoform-specific knockouts dissociate these opposing transcriptional activities, highlighting features that are dispensable for transactivation but critical for repression and for proper germ cell formation. Together, these results demonstrate that certain p53 isoforms function as constitutive tissue-specific repressors, raising important implications for tumor suppression by the human counterpart.

INTRODUCTION

The p53 gene is altered in most human cancers, and oncogenesis often requires normal p53 function to become disabled or deranged (Soussi and Wiman, 2015). A prevailing model is that, in response to stress, transcriptional induction of target genes by p53 promotes apoptosis, cell cycle arrest, or senescence (reviewed in Vousden and Lane, 2007). However, p53 variants decoupled from these pathways retained tumor suppressive functions (Brady et al., 2011; Li et al., 2012), and likewise, the combined elimination of canonical target genes (p21, noxa, and puma) also produced tumor-free animals (Valente et al., 2013), suggesting that p53 can restrain cancers without canonical effectors (Brady et al., 2011; Li et al., 2012). The need for stimulus-dependent regulators has been similarly debated, and although Chk2 is typically required for p53 transactivation, cancer susceptibilities in mouse models and *Li Fraumeni* patients indicate that p53 directs tumor suppression independent of this upstream kinase (Takai et al., 2002; Ruijs et al., 2009). Taken together, these observations raise the possibility that unappreciated processes, independent of Chk2, are important for p53-mediated tumor suppression.

p53 is a transcription factor that directly binds to chromatin and induces the expression of target genes (Beckerman and Prives, 2010; Brodsky et al., 2000). The canonical p53 DNA binding motif (p53 DBM) consists of two tandem copies of the decamer motif "RRRCWWGYYY," where "R" represents purines, "W" represents adenine or thymine, and "Y" represents pyrimidines (El-Deiry et al., 1992). The p53 protein is comprised of three domains, an N-terminal transactivation domain (TAD), a central DNA binding domain (DBD), and a C-terminal oligomerization domain (OD) (Brodsky et al., 2000; Vousden and Lane, 2007). Since most p53 missense mutations in human cancers reside in the DBD, it seems that DNA binding is critical for p53 tumor suppression (Soussi, 2007).

p53 action also downregulates genes, and this phenomenon is commonly observed in cell culture and *in vivo* model systems (Fischer, 2017; Akdemir et al., 2007; Tanikawa et al., 2017). However, gene repression by p53 is generally assumed to reflect secondary consequences that are indirect and downstream of transcriptional activation (Sullivan et al., 2018). After stress, for example, p53 indirectly downregulates cell cycle genes by transcriptionally activating p21/CDKN1A that inhibits cyclin-dependent kinases through the DREAM (DP, RB-like, E2F4 and MuvB) complex (Fischer et al., 2016). p53 can also downregulate genes by promoting expression of microRNAs (miRNAs) or long non-coding RNAs (lncRNAs) (Feng et al., 2011; Chaudhary and Lal, 2017). Reports of p53 downregulation also involve occlusion of the transactivators and/or the association with co-repressors (Chaudhary and Lal, 2017; Wang et al., 2010), but whether direct p53 occupancy on chromatin acts to repress target genes *in vivo* is a long-standing controversy in the field (Sullivan et al., 2018).

Tissue-specific and pleiotropic responses by p53 could be dictated by different p53 isoforms since throughout the animal

kingdom, p53 genes generate alternatively spliced transcripts encoding proteins that either retain or lack the TAD (Marcel et al., 2011). For example, *Drosophila* p53 encodes three distinct isoforms that differ at the N-terminal TAD. Similarly, the human p53 gene encodes a full-length protein and three truncated N-terminal isoforms that partially or fully lack the TAD. Additional complexities are encoded by human p53, since alternate splicing at the C terminus generates three OD variants. These isoforms are expressed in a wide range of normal tissues (Khoury and Bourdon, 2010), and since the central DBD is shared by all p53 isoforms, hotspot cancer point mutations could presumably affect all encoded p53 proteins (Marcel et al., 2011). Furthermore, p53 protein isoforms can either homo- or hetero-oligomerize to promote transcriptional outputs (Khoury and Bourdon, 2011). Therefore, only a subset of isoforms may be needed for tumor suppression, or alternatively, multiple isoforms could be involved.

To better understand mechanisms of p53 gene downregulation, we characterized *in vivo* biosensors that report repression by p53 in the *Drosophila* system. Surprisingly, these same biosensors report gene activation by p53 earlier in development (Lu et al., 2010; Wylie et al., 2014). Therefore, using these tools, we examined how p53 codes for opposing transcriptional outcomes at a well-defined target and at native genomic sites. Through sufficiency testing and loss-of-function studies, we found that certain p53 isoforms function as constitutive repressors, raising the possibility that competition among repressive and activating isoforms could produce distinct transcriptional outputs. Since the human counterpart codes for similar isoform variants, these findings have important implications for understanding tumor suppression by p53.

RESULTS

A p53 biosensor tracks stimulus-dependent induction and basal transrepression

We authenticated a series of *in vivo* biosensors that visualize stimulus-dependent p53 transactivation in live *Drosophila* embryos (Lu et al., 2010). These biosensors, designated p53R-GFP (Green Fluorescent Protein), were not only conditional upon stress and p53 (Table S1; Figures S1A–S1A″), but they also disclosed evidence of tissue-specific post-translational regulation (Figures S1B and S1C). For example, despite considerable expression of p53 protein in neuronal precursors, stimulus-dependent p53 action was clearly absent from these cells (Figures S1B and S1C), and in follow-up studies, we found surprising evidence for p53-mediated repression. Figure 1 illustrates a prominent example of this activity seen in 3rd instar larvae. Here, p53R-GFP expression was robust in the salivary glands of p53^{-} nulls but nearly absent in wild-type (WT) animals or p53 mutant counterparts carrying a p53 rescue transgene. Importantly, both nuclear (Figures 1A and 1C) and cytoplasmic (Figures 1B and 1C) variants of the biosensor showed concordant p53-dependent repression, and moreover, signals were readily detected in live as well as fixed preparations (Figures S1D–S1D‴). This repressive activity was also autonomous, since identical outcomes occurred when p53 was silenced using RNAi in salivary glands (Figure S1E) and, unlike embryonic tissue, p53R-GFP was not radiation responsive in this organ (Figure S1F). Furthermore, p53 repressive activity was not restricted to this stage of development and, notably, could be observed in diverse first instar larval tissues as well as adult digestive organs (Figures S1G–S1K′). Collectively, these results show that a single p53 biosensor can be used to visualize p53 stimulus-dependent transactivation and p53 transrepression in distinct developmental stages and tissues (Figure 1D). Both activities occurred irrespective of biosensor transgene position and were retained in three independent genomic insertions (Figures S1L–S1N‴; Table S1). Importantly, unlike stimulus-dependent p53 activity seen in Figure S1, p53 repression seen here is constitutive and does not require exposure to a stressor.

p53 transactivation and transrepression are genetically distinct

Chk2 is an evolutionarily conserved serine/threonine kinase that is activated in response to DNA damage (Ahn et al., 2004). Like its mammalian counterpart, *Drosophila* Chk2 directly phosphorylates p53 (Hirao et al., 2000; Peters et al., 2002) and is important for stimulus-dependent p53 activity (Peters et al., 2002; Lu et al., 2010; Wylie et al., 2014). Consistent with this, as seen in Figures 2A–2C, stimulus-dependent p53 transactivation completely fails in Chk2 mutants after irradiation. Therefore, we asked whether constitutive transrepression mediated by p53 also required Chk2, and in contrast to p53^{-} glands, p53R-GFP repression was unaffected in Chk2^{-} salivary glands (Figures 2D–2F). Furthermore, p53R-GFP biosensor derepression in Chk2^{-};p53^{-} double mutants was indistinguishable from single p53^{-} mutant counterparts, demonstrating that Chk2 function is fully dispensable for biosensor repression (Figures S2A–S2D′). Identical patterns were observed using other biosensor insertions, thus excluding position effects (Figures S2E–S2E″). Furthermore, the effect was not salivary gland specific, as p53 biosensor repression was clearly Chk2 independent in other tissues as well (Figures S2F–S2H′). Hence, the opposing transcriptional activities mediated by p53 are genetically distinct and operationally defined by Chk2 dependence.

p53 transrepression and transactivation are mediated through a single DNA binding element

Fly and human p53 proteins bind virtually identical DNA motifs, referred to here as the p53 DBM (see Figure 3A‴) (Brodsky et al., 2000; Wang et al., 1995). To ask whether p53 transactivation and p53 transrepression occur through this same canonical *cis* element (Figure 3A), we targeted the p53 biosensor using CRISPR-Cas9 editing and recovered several strains with deletions or indels at the p53 DBM. As shown in Figure 3, stimulus-induced biosensor expression required an intact p53 DBM (Figures 3B–B‴; Table S2). Likewise, constitutive repression by p53 also required the DBM, since this was completely abolished in animals harboring DBM deletions (Figures 3C–3C‴). We observed similar results when the p53DBM was cleanly deleted at an additional genomic position (Figures S3A–S3B′). Taken together, these observations establish that p53 transactivation and p53 transrepression are both mediated through a canonical DNA element (Figure 3; Figure S3; Table S2). Furthermore, smaller indels within the p53 DBM also impacted biosensor repression and transactivation, indicating that both half-site sequences within the DBM are necessary for efficient p53 action (Figures S3C–S3H).

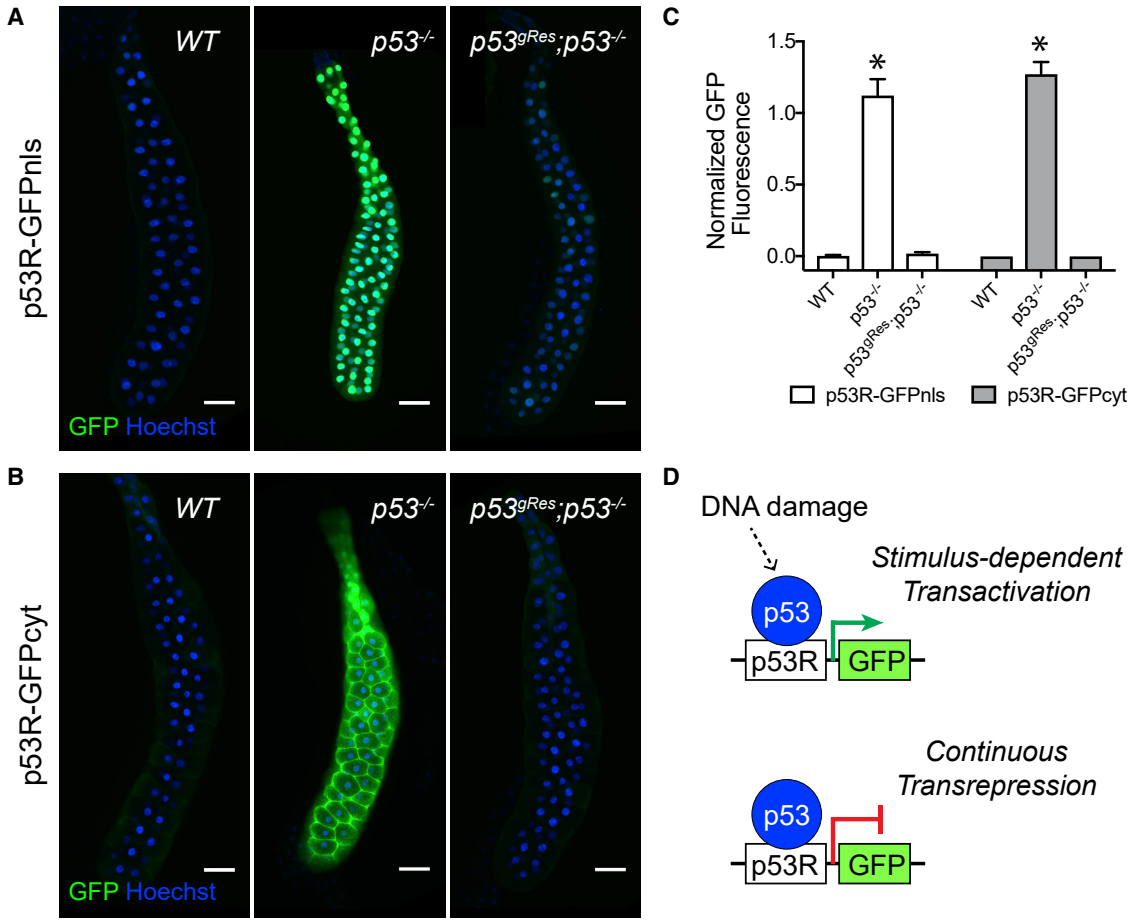

Figure 1. p53 biosensors report constitutive transrepression in post-embryonic tissues

(A) Robust p53R-GFPnls activity in the salivary glands of p53^{-} 3rd instar larvae (middle panel) is effectively repressed in WT (left panel) and likewise also absent in p53^{-} animals rescued with a p53 transgene (p53^{gRes};p53$^{-/-}$, right panel) (Wylie et al., 2016). Salivary glands were immunostained for GFP (green) and counterstained for Hoechst (blue). Scale bars, 100 μm.

(B) Similar patterns are observed with the p53R-GFPcyt biosensor (see methods), where robust GFP expression seen in p53^{-} animals (middle panel) is repressed in WT and p53 genomic rescue strains. Scale bars, 100 μm.

(C) Patterns in (A) and (B) are quantified in (C) where GFP fluorescence was normalized to Hoechst staining. Error bars represent standard deviations from three biological replicates. p53^{-} was significantly different from wild type (*p value < 0.0001) and p53^{gRes};p53^{-} (*p value < 0.0001) for both biosensor transgene positions.

(D) Schematic illustrating how p53 biosensors report stimulus-dependent transactivation (Figure S1) and constitutive transrepression (Figure 1).

p53 repression occurs through direct binding to canonical DNA sites

Results in Figures 3C–3C‴ suggested that p53 transrepression operates through direct occupancy of the canonical p53 DBM in the p53R-GFP transgene. Therefore, we used cleavage under targets and release using nuclease (Cut&Run) (Skene and Henikoff, 2017) to examine chromatin occupancy in salivary glands using a p53-mCherry-tagged genomic rescue construct in p53^{-} animals (p53^{mCh}), which is functionally WT (Zhang et al., 2014). We first interrogated Cut&Run reads uniquely assignable to the p53R-GFP biosensor since the p53 regulated enhancer is also present natively in the fly genome (Brodsky et al., 2000). As shown in Figures 3D and 3D′, p53^{mCh} binding signals were present at the p53 biosensor and, importantly, were absent from both p53^{-} flies and from p53R-GFPΔDBM flies, which lack the p53 DBM but express p53^{mCh} (Figures 3D and 3D′). Furthermore, canonical target genes (e.g., *xrp1*) were similarly bound by p53^{mCh} flies, irrespective of biosensor status (Figures 3E and 3E′; Figure S3J; Kurtz et al., 2019a). Binding profiles from Cut&Run reads mapping to either the biosensor or the native *reaper* locus were also consistent with this (see Figures S3I and S3K). To extend these findings, we similarly used Cut&Run to profile p53-dependent histone marks. Elevated H3K9me3 (a repressive mark) and decreased H3K4me3 (an activating mark) correlated with p53 occupancy and p53 dependent repression at the biosensor (Figures 3D′–3D‴). In contrast, H3K4me3 and H3K9me3 profiles were unchanged at a transactivated target, *xrp1* (Figures 3E″ and 3E‴), and consistent with this, we confirmed that *xrp1* expression is unaffected by p53 status in salivary glands (Figure S4J′). Therefore, p53 binds—and possibly directs—H3K9me3 repressive chromatin marks at the p53 biosensor (Figure 3; Figure S3). Since the p53 motif here matches the human consensus site (Figure 3)A‴, the findings raise the possibility that human p53 may similarly

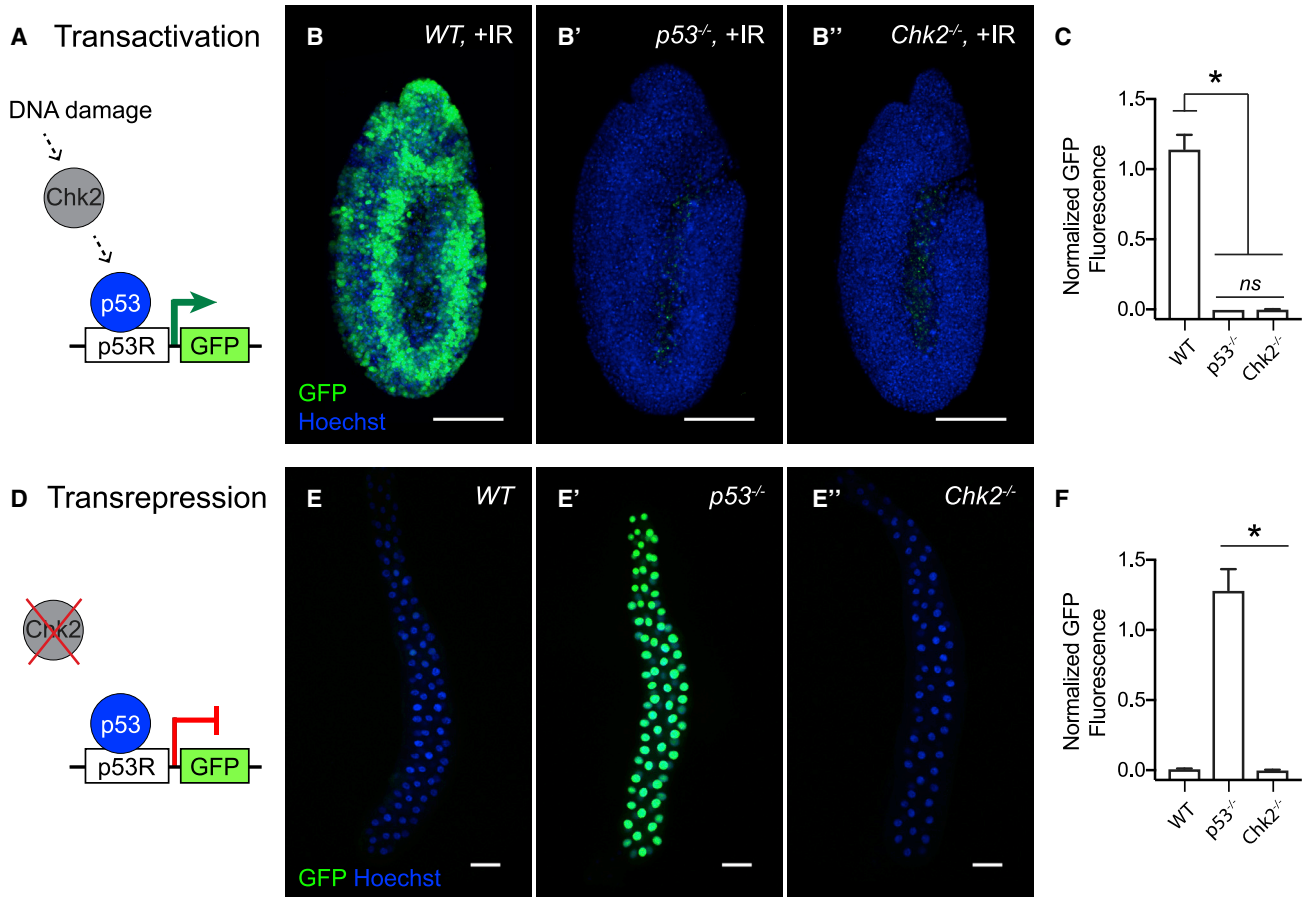

Figure 2. Chk2 is required for p53 transactivation but not for p53 transrepression

(A–C) Chk2 is required for stimulus-dependent p53 transactivation. (A) Chk2 phosphorylates p53 to promote p53 transcriptional activation of target genes after radiation exposure (Hirao et al., 2000; Peters et al., 2002). Irradiated WT (B), p53^{-} (B′), and Chk2^{-} (B″) embryos carrying the p53R-GFPnls biosensor transgene were immunostained for GFP (green) and counterstained with Hoechst (blue). Note that induced biosensor activity in WT (B) is completely abolished in p53^{-} (B′) and Chk2^{-} (B″) animals. Patterns in (B)–(B″) are quantified in (C) where GFP fluorescence was normalized to Hoechst staining. p53^{-} and Chk2^{-} embryo transactivation is not significantly different (ns). Error bars represent standard deviations from three biological replicates. Biosensor induction in WT animals is significantly different from Chk2^{-} and p53^{-} animals (*p value < 0.0001). Scale bars, 100 μm.

(D–F) Constitutive transcriptional repression by p53 is Chk2 independent. The p53R-GFPnls biosensor is effectively repressed in WT (E) and Chk2^{-} animals (E″) but de-repressed in p53^{-} animals (E′). Glands were immunostained for GFP (green) and counterstained for Hoechst (blue). Patterns in (E–E″) are quantified in (F) where GFP fluorescence was normalized to Hoechst staining. Error bars represent standard deviations from three biological replicates. WT and Chk2^{-} glands are equivalent and p53^{-} glands are significantly different from both (*p value < 0.0001). Scale bars, 100 μm.

operate as a constitutive transcriptional repressor at canonical p53DBMs.

Distinct p53 isoforms code for opposing transcriptional outcomes

p53 genes throughout the animal kingdom generate alternatively spliced transcripts that lack the TAD (Marcel et al., 2011). Importantly, all retain the DBD, suggesting that certain p53 isoforms could act on chromatin without inducing target genes. In *Drosophila*, the p53 locus encodes three distinct isoforms two of which lack a complete activation domain and could plausibly function as transcriptional repressors (Figure 4A). To test this hypothesis, we methodically assessed isoform activity by targeting mCherry fusions of each to p53^{-} salivary glands and visualizing their impact on the biosensor (Figures 4B and 4B′; Table S3). In these sufficiency assays, the p53A or p53E isoforms clearly functioned as transrepressors. In contrast, the p53B isoform conferred robust transcriptional activation, and moreover, mCherry alone did not significantly impact biosensor activity. In these addback studies, we also assessed expression levels (Figure 4B″; Figure S4) and found, importantly, that p53B and p53A were present at comparable levels. Thus, in these assays, expression levels did not determine whether a given isoform qualifies as transactivator or transrepressor (Figure 4; Figure S4). In addition, we found no evidence for ectopic cell death in the salivary glands of these animals (Figure S4), consistent with previous reports that these tissues are resistant to cell death at this stage (Zhang et al., 2014).

p53 isoform-specific loss-of-function alleles expose surprising complexities

We next assessed p53 isoform function by loss-of-function analyses, and we used CRISPR-Cas9 editing to individually

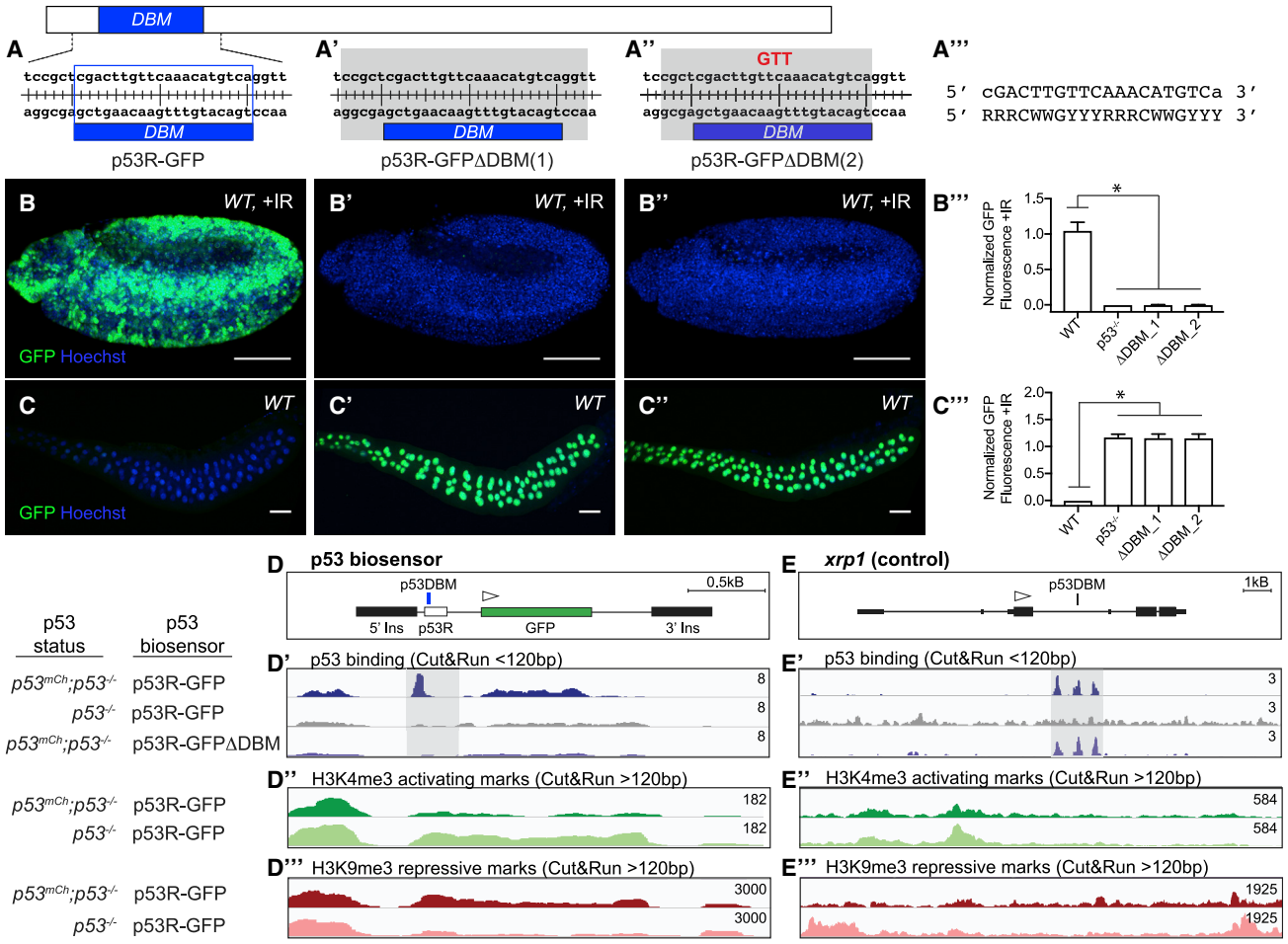

Figure 3. p53 repression is mediated through a canonical p53 DNA binding motif

(A–C) (A) The 150 bp genomic regulatory fragment within the p53 biosensor (white box) contains a canonical 20 bp p53 binding element, labeled DNA binding motif (DBM) (blue box, see STAR Methods). When the DBM is intact (A–C), these biosensors effectively report p53-mediated transactivation in irradiated embryos (B) and transrepression in 3rd instar salivary (C). p53 biosensor is in green (GFP) and nuclei are counterstained with Hoechst (blue). All scale bars represent 100 μm.

(A′–C′) A targeted 28-bp deletion (see methods) spanning the DBM (gray box in A′) completely abolishes radiation-dependent biosensor transactivation (B′) and transrepression in salivary glands (C′) in animals that are wild type for p53. (A″–C″) Similarly, *WT* animals harboring an indel at the DBM (see STAR Methods), consisting of a 24-bp deletion (gray box) and GTT insertion (red letters) (A″), fail to transactivate (B″) and fail to transrepress (C″) in respective tissues. (A‴) The p53 biosensor DBM (top line) matches the human consensus (bottom line) but diverges at the two most terminal nucleotides (top line, lower case letters). The human consensus consists of two adjacent 10-mers where R is purine, Y is pyrimidine, and W is either A or T (El-Deiry et al., 1992). (B‴) Stimulus-dependent transactivation in (B–B″) is quantified in (B‴), where GFP was normalized to the Hoechst signal. p53 and DBM status are annotated below. Error bars represent standard deviations from three biological replicates. *WT* animals that carry an intact DBM are significantly different from animals that are p53^{-} or have the DBM deleted (*p value < 0.0001). (C‴) Constitutive transrepression in (C)–(C″) is quantified in (C‴), where GFP was normalized to the Hoechst signal. p53 and DBM status are annotated below. Error bars represent standard deviations from three biological replicates. *WT* animals that carry an intact DBM are significantly different from animals that are p53^{-} or have the DBM deleted (*p value < 0.0001).

(D and E) (D–E‴) p53 Cut&Run seq (D′ and E′), H3K4me3 Cut&Run seq (D″ and E″), and H3K9me3 Cut&Run seq (D‴ and E‴) were performed in *p53^{mCh};p53^{-}* 3rd instar salivary glands and tracks are shown for the p53 biosensor (D–D‴) and a control region, *xrp1* (E–E‴). (D) Illustration of the biosensor, where p53R is the p53 responsive fragment (white box) that contains the p53DBM (blue box) (Brodsky et al., 2000) and (E) illustration of the *xrp1* gene with exons indicated. Arrowheads indicate the direction of transcription. Scale bar is noted in the upper right corner of (D) and (E), and panel heights in normalized read counts are shown in the upper right corners of (D′)–(E‴).

(D′ and E′) p53 Cut&Run seq was performed in p53^{mCh};p53^{-} salivary glands using a dsRed antibody. Genotypes and biosensor status are noted on the left, and relevant binding peaks are shaded in gray (D′ and E′). Binding observed in (D′) requires p53 and an intact p53 DBM as signals in WT (dark blue reads) are absent in p53^{-} (gray track) and in p53R-GFPΔDBM (light blue reads). (D′) As expected, p53 was bound to *xrp1*, irrespective of biosensor status. Unique and multimapped Cut&Run reads to the biosensor are provided in Figure S3.

(D″ and E″) Cut&Run experiments measuring H3K4me3-activating chromatin marks in p53^{mCh};p53^{-} (dark green) and p53^{-} salivary glands (light green). Note: elevated H3K4me3 marks correlate with loss of p53 binding at the p53 biosensor (D″) but not at the *xrp1* locus (E″).

(D‴ and E‴) Cut&Run experiments measuring H3K9me3 repressive chromatin marks in p53^{mCh};p53^{-} (dark red reads) and p53^{-} salivary glands (light red reads). Note: elevated H3K9me3 marks correlate with p53 binding at the p53 biosensor (D‴) but not at the *xrp1* locus (E‴).

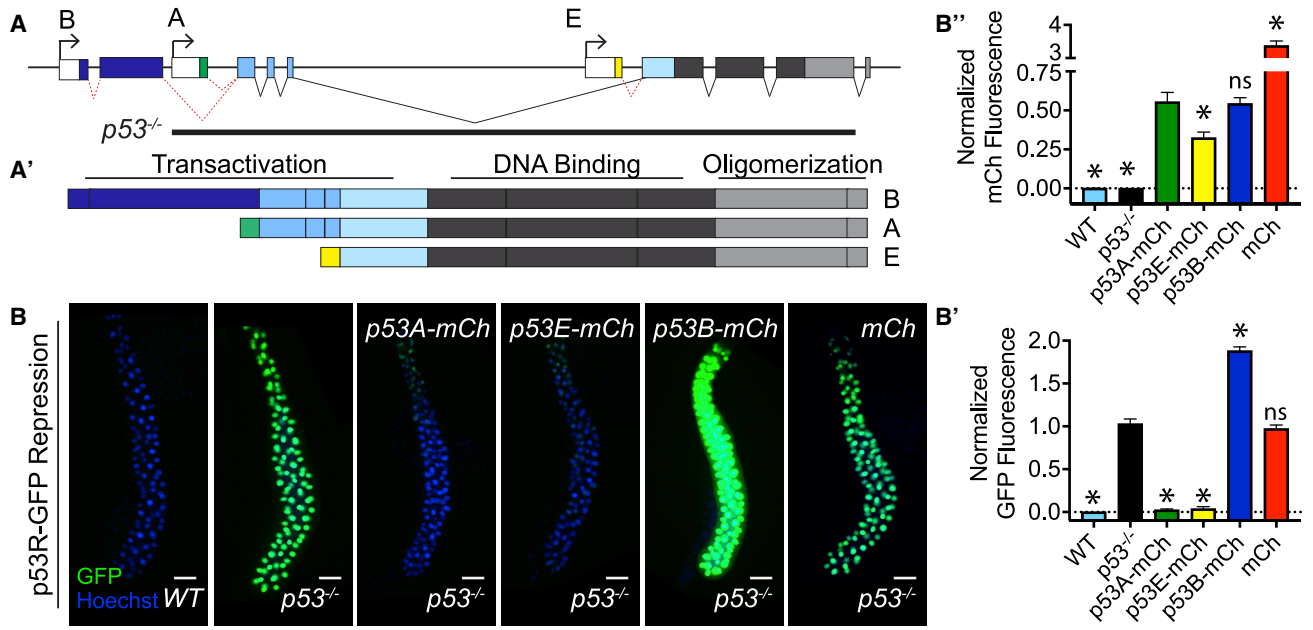

Figure 4. Distinct p53 isoforms code for opposing transcriptional outcomes

(A) (A and A′) *Drosophila* p53 encodes three p53 isoforms that differ at the N-terminal transactivation domain. (A) Diagram of the *Drosophila* p53 gene region where lines represent introns and boxes represent exons. Note that the p53^{-} deletion (black line) is a null allele for all isoforms (Xie and Golic, 2004). Alternate splicing and alternate promoter usage leads to three p53 isoforms (A′) that differ at the transactivation domain (dark blue, green, and yellow boxes) but share a DNA binding (dark gray) and oligomerization domain (light gray). In addback experiments (B–B″), mCherry fusions of each isoform were independently expressed and tested in salivary glands of p53 null animals.

(B) Distinct p53 isoforms produce opposing transcriptional outcomes. Targeted expression of either the p53A (third panel) or p53E (fourth) in p53^{-} animals effectively repress the biosensor to near WT levels (first panel). Conversely, targeted salivary gland p53B-mCh expression (fifth panel) leads to elevated p53R-GFP expression when compared with p53^{-} (second panel) and targeted mCherry control animals (sixth panel). Salivary glands are counterstained with Hoechst (blue). Scale bars, 10 μm. p53 biosensor activity shown in (B) is quantified in (B′), where GFP was normalized to the Hoechst signal. Error bars represent standard deviations from three biological replicates. WT, p53B-mCh, p53A-mCh, and p53E-mCh targeted expression animals are significantly different from p53^{-} animals (*p value < 0.0001). mCherry-targeted expression control animals are not significantly different from p53^{-} animals (ns). (B″) Quantifies targeted p53 expression in these salivary glands by immuno-detection of mCherry normalized to Hoechst signal (Figures S4B–S4G′). Error bars represent standard deviations from three biological replicates. Note that expression of p53B-mCh is similar to expression of p53A-mCh in these addback animals (ns) but have opposing transcriptional outcomes (B′ and B″). Representative images of mCherry expression are provided in Figure S4. p53B-mCh animals are not significantly different from p53A-mCh animals (ns). WT, p53^{-}, mCh, and p53E-mCh animals are significantly different from p53A-mCh and p53B-mCh animals (*p value < 0.0001).

eliminate each p53 isoform. Specifically, we captured isoform-specific null alleles and sequence-verified each alteration, as indicated in Figure S5A. In addition, we verified that for each knockout, the remaining isoforms were undisturbed, and hence, corresponding phenotypes can be assigned to the isoform in question (Figures S5B–S5B″). Next, we visualized our p53 biosensors in animals homozygous for each of these alleles. As shown in Figure 5, mutants lacking either p53B and p53E isoforms each retained full transrepressive activity but mutants lacking the p53A isoform completely failed to repress GFP and phenocopied p53 loss in this assay. Hence, a single isoform, p53A, was necessary for transrepression in the salivary gland (Figures 5A and 5A′). We also examined requirements for each p53 isoform in a model of stimulus-induced p53 transactivation, whereby germline stem cells (GSCs) are monitored after radiation challenge (Wylie et al., 2014). In these assays, we found the converse pattern. Specifically, the p53B isoform, was required for p53 biosensor transactivation and the p53A isoform was clearly dispensable (Figures 5B and 5B′; Figures S5C and S5C′). Notably, although p53E has the capability to act as a repressor in sufficiency assays (Figure S4B), we detected no clear role for this isoform in these loss-of-function studies (Figures 5A–5C′). Outcomes from the salivary gland addback assays (Figure 4) and loss-of-function studies (see Figures 5A–5C′) together with evidence below (Figures 6 and 7) suggested that p53A could be a dedicated transrepressor. However, additional complexities emerged as we examined irradiated embryos since, here, the p53A isoform was essential for transactivation, whereas the p53B and p53E isoforms were dispensable (Figures 5C and 5C′; Tables S3 and S4). Further complexity was seen in irradiated ovaries where p53 activity is normally restricted to the GSCs of WT animals (see Wylie et al., 2014 and Figure 5D). However, in p53A knockouts, the p53 biosensor reported widespread, ectopic activity in somatic ovarian cells which, notably, was fully abolished when all p53 isoforms were missing (Figures 5D and 5D′). Importantly, this ectopic activation was radiation-dependent and replicated in independent p53A alleles (Figure S5D). Therefore, in the ovary, p53A is a pivotal factor that restricts damage-induced activity to the ovarian stem cell compartment. Furthermore, since ectopic p53R-GFP was lost when all isoforms were absent, the results could indicate that repression by p53A constitutively prevents the activating p53B

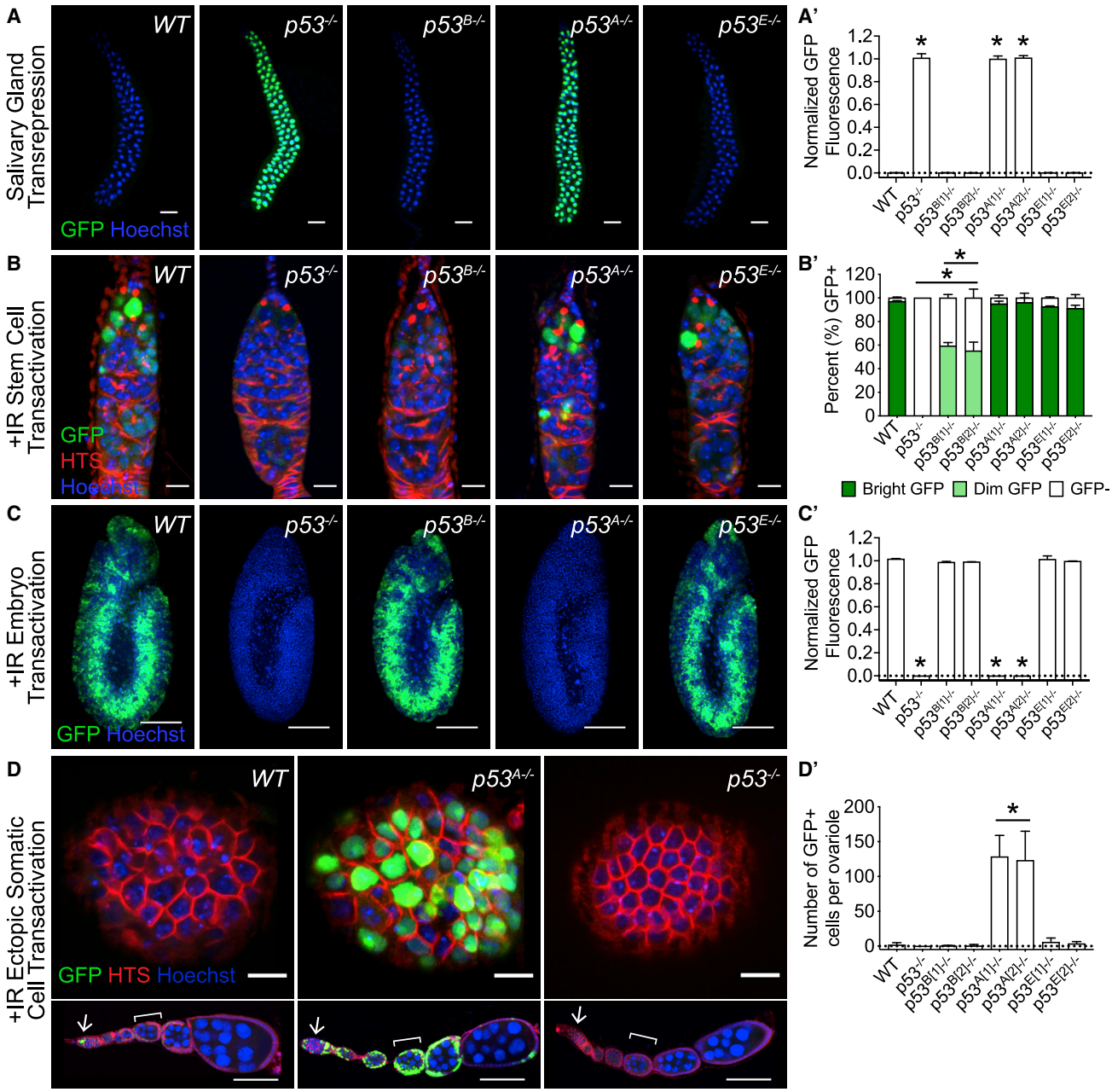

Figure 5. Isoform-specific knockouts reveal complex interactions

(A) (A and A′) p53A knockouts phenocopy loss of all p53 isoforms (p53^{-}) with robust GFP derepression observed in salivary glands. This derepression was not observed in p53B knockouts or p53E knockouts. Representative images of p53 biosensor activity (green) are shown in (A) and quantification is graphed in (A′). Salivary glands in (A) are counterstained with Hoechst (blue) bars, 100 μm. Error bars in (A′) represent standard deviations from three biological replicates. p53^{-}, p53$^{A[1]\,-}$, and p53$^{A[2]\,-}$ alleles are significantly different from WT animals (*p value < 0.0001).

(B) (B and B′) The p53B isoform is required for efficient p53 biosensor transactivation in the germline stem cell compartment. Representative images (B) and quantification (B′) from isoform-specific p53 knockouts. p53 biosensor activity (green) and nuclei are counterstained with Hoechst (blue). Germline stem cells and cystoblast daughters can be identified by the rounded fusome stained with HTS ((hu li tai shao) (red). Scale bars, 10 μm. Note that p53 biosensor transactivation is significantly abolished in two independent p53B isoform-specific alleles (*p value < 0.0001) but not to the full extent seen in p53^{-} deletion flies (*p value < 0.0001), over three biological replicates.

(C) (C and C′) The p53A isoform is required for p53 biosensor transactivation in irradiated embryos. Representative images (C) and quantification (C′) from isoform-specific p53 knockouts. p53 biosensor activity (green) and nuclei are counterstained with Hoechst (blue). Scale bars, 100 μm. Error bars in (C′) represent standard deviations from three biological replicates. Note that p53 biosensor transactivation is abolished in p53^{-} animals (lacking all isoforms) and two independent p53A knockouts, one of which is shown here (*p value < 0.0001) but is unaffected p53B knockouts and p53E knockouts.

(D) (D and D′) p53A knockouts are specifically permissive for ectopic p53 activity. In somatic cells of irradiated ovaries, the p53 biosensor is unresponsive in WT animals (D, upper left panel) but acutely responsive in p53A knockout alleles (D, upper middle panel). Below are low magnification images of ectopic activity

(legend continued on next page)

isoform from operating on the DBM in the p53 biosensors (Figures S5D′ and S5D″). Hence, these data raise the possibility that competition among repressive and activating p53 isoforms may contribute to tissue-specific outputs.

The meiotic gene, *corolla*, is a target of p53 repression

To ask whether direct p53 repression occurs at native genes, we surveyed existing datasets (Kurtz et al., 2019a), and as a case study, we interrogated the *corolla* locus, which encodes a component of the synaptonemal complex (Collins et al., 2014). As seen in Figure 6, p53 clearly binds the promoter region of this gene (Figures 6A and 6B; Figure S6), and furthermore, p53 occupancy tightly correlated with the presence of repressive H3K9me3 chromatin marks (Figure 6C). Importantly, *corolla* transcripts were dramatically elevated in $p53^{-}$ ovaries (Figures 6B and 6D), and consistent with this, activating H3K4me3 marks was similarly elevated in p53 mutants (Figure S6). Notably, these effects occurred without the need for stress or Chk2 and were reversed in $p53^{-}$ animals carrying a p53 genomic rescue transgene (Figures 6D and 6E). Together, these data suggest that p53 constitutively binds and specifies *corolla* repression. To ask whether this was a direct regulatory effect, we used CRISPR-Cas9 editing to produce animals deleted for a putative p53DBM at the *corolla* locus (Figure 6A; Figure S6A). As shown in Figure 6F, animals deleted for this p53DBM (red triangle in Figure 6A) were strikingly derepressed when tested for *corolla* expression, and in effect, these mutants phenocopied *corolla* levels seen in $p53^{-}$ animals. Thus, a regulatory site normally bound by p53 exerts constitutive repression on a native target. We note that another computed DBM (not tested here) could potentially exert similar and/or cooperative activity, since authentic p53 binding signals were also detected nearby this upstream site (open triangle in Figure 6A).

We next tested whether a distinct isoform might be dedicated to *corolla* repression. In these assays, *corolla* transcript levels were unaffected in p53B and p53E knockouts but were highly elevated when independent p53A knockouts were inspected (Figure 6G). Thus, the p53A isoform is responsible for *corolla* repression (Figure 6G; Table S3). To examine precisely where in the ovary p53 acts to repress *corolla*, we performed immunostaining in $p53^{mCh}$ genomic rescue animals and observed that p53 protein specifically accumulates in the early oocyte (Figure 6H). Notably, Corolla was also present in these cells but became markedly elevated in animals harboring either a complete p53 knockout or a p53A isoform-specific allele (Figures 6I–6I″; Figure S6). Taken together, these data indicate that in the early oocyte, p53A is a constitutive repressor of *corolla*. Importantly, this effect was mediated through a canonical p53 DBM (Figure 6F) and occurred without the need for Chk2 (Figure 6E). Hence, features of p53 transcriptional repression that were exposed using our biosensors clearly extend to endogenous genes.

A unique allele disassociates transrepression and transactivation

Figures 4, 5, and 6 show that the p53B isoform is a dedicated transactivator, and the p53A isoform can function as either a repressor or activator (see Table S3 summary). To understand how a single isoform encodes opposing transcriptional activities, we characterized a unique in-frame deletion allele, designated $p53^{A\Delta5}$. This lesion specifically removes 5 amino acids from the p53A isoform (see Figure 7A) and, importantly, leaves expression levels of all isoforms unperturbed (Figure S7). When combined with p53 biosensors, the $p53^{A\Delta5}$ allele was completely defective for transrepression in the salivary gland and, in effect, phenocopied $p53^{-}$ animals (Figures 7B and 7B′). Surprisingly, however, these same $p53^{A\Delta5}$ animals were completely normal for stimulus-dependent transactivation when tested as embryos (Figures 7C and 7C′). In related experiments, we excluded the possibility that p53R-GFP is simply derepressed in all $p53^{A\Delta5}$ tissues (Table S5). Together, the results in Figures 7B–7C′ show that opposing transcriptional p53 activities can indeed be uncoupled, highlighting five amino acids that are critical for repression but dispensable for transactivation.

Next, we tested whether dissociating properties of the $p53^{A\Delta5}$ allele also extended to native genes. In embryos, the cell death gene, *reaper*, is a well-characterized direct target that exhibits acute, p53-dependent induction following DNA damage (Brodsky et al., 2000). Therefore, we profiled irradiated embryos for *reaper* induction and found that p53A knockouts were completely defective for this response (Figure S7). However, in contrast, $p53^{A\Delta5}$ mutants were fully normal for *reaper* induction (Figure 7D), as were animals lacking either p53B or p53E (Figure S7; Table S3). Consistent with this, $p53^{A\Delta5}$ embryos were also normal for irradiation-induced apoptosis, in stark contrast to $p53^{-}$ animals (Figure 7D′; Akdemir et al., 2007). Taken together, these findings definitively attribute *reaper* induction and the associated biologic response (cell death) to transcriptional activation mediated by the p53A isoform.

Repression by p53A is needed for proper germ cell formation

Since $p53^{A\Delta5}$ animals are selectively defective for repression imposed by p53, we used these mutants to investigate the biological relevance of this activity. Like $p53^{-}$ ovaries, *corolla* transcripts and Corolla protein were profoundly derepressed in $p53^{A\Delta5}$ animals (Figures 7E and 7E′). This dysregulation persisted through later developmental stages since ectopic Corolla clearly endured in the primordial germ cells (PGCs) of $p53^{A\Delta5}$ embryos (Figure S7). Defective PGC numbers had been previously reported in $p53^{-}$ animals (Tarayrah-Ibraheim et al., 2021; Yamada et al., 2008), and accordingly, we profiled our alleles for equivalent PGC phenotypes. As seen in Figures 7F–7G′, knockouts for p53B and p53E were normal for PGCs, but animals lacking p53A or mutant for the $p53^{A\Delta5}$ allele notably phenocopied $p53^{-}$. Therefore, proper PGC development requires

(green) in ovarioles. Brackets indicate the stage of egg chamber imaged above and arrows indicate the stem cell compartment. Ovaries are counterstained with HTS (red) and Hoechst (blue). Scale bars, 10 (above) and 100 μm (below). When all p53 isoforms are removed, ectopic activity is abolished (D, right panel, D′), indicating that p53 isoforms other than p53A induce the biosensor. (D′) Quantification of ectopic activity with numbers of GFP positive cells per ovariole graphed. Error bars represent standard deviations from 48 to 179 biological replicates. Two independent p53A isoform-specific knockout alleles are significantly different from all other genotypes (*p value < 0.0001). p53B knockouts and p53E knockouts are identical to WT and non-permissive for ectopic activity.

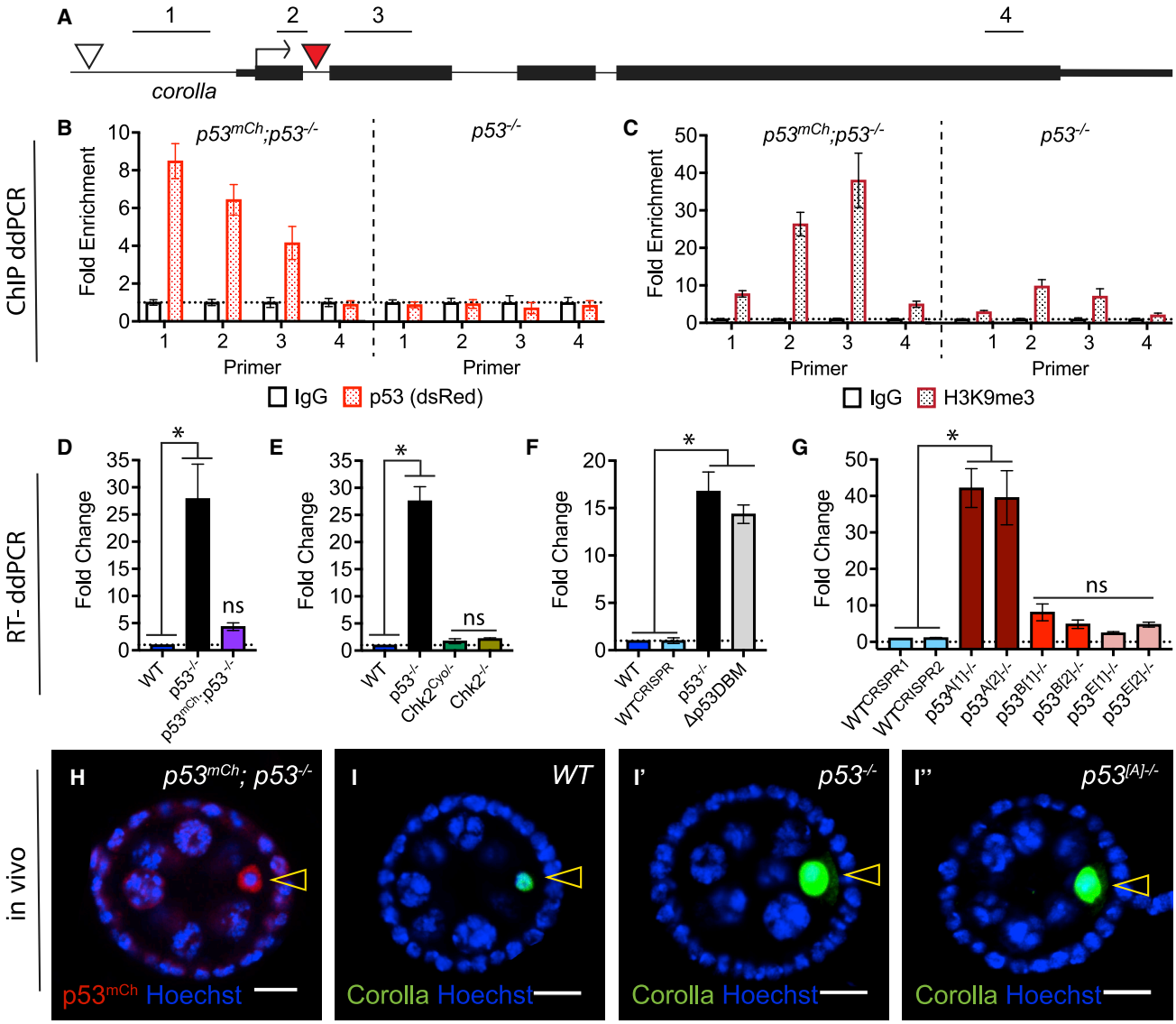

Figure 6. The meiotic gene *corolla* is a direct target of p53 repression

(A) The *corolla* locus, where thick boxes represent exons, thick lines represent untranslated regions, thin lines represent introns, and gray thin lines represent extended gene regions. Triangles denote computationally predicted p53 DNA binding motifs, where the targeted p53DBM deletion in (F) is designated in red (see Figure S6). Numbered lines represent primer amplicons used in ChIP-ddPCR (chromatin immunoprecipitaiton droplet digital polymerase chain reaction) for (B) and (C).

(B) p53 binds the *corolla* promoter region. ChIP-ddPCR experiments measuring $p53^{mCh}$ occupancy using a dsRed antibody (red bars) in $p53^{mCh}$;$p53^{-}$ (left) and $p53^{-}$ ovaries (right) at indicated amplicons through the *corolla* gene region. Genotypes, separated by a dotted line, are indicated with amplicons shown in (A) listed on the x axis. Values represent fold enrichment over immunoprecipitation with control IgG (white bars). Positive and negative control regions are included in Figure S6. Error bars represent confidence intervals and an additional biological replicate is provided in Figure S6B.

(C) H3K9me3 repressive marks correlate with p53 binding at *corolla*. ChIP-ddPCR experiments measuring H3K9me3 repressive chromatin marks (dark red shaded bars) in $p53^{mCh}$;$p53^{-}$ (left) and $p53^{-}$ ovaries (right) at the *corolla* gene region. Values represent fold enrichment over immunoprecipitation using IgG (white bars). Error bars represent confidence intervals and an additional biological replicate is provided in Figure S6C.

(D) p53 inhibits *corolla* expression in the ovary. RT-ddPCR (reverse transcriptase droplet digical polymerase chain reaction) analyses show that *corolla* expression is derepressed in $p53^{-}$ ovaries (black bar) and reversed in $p53^{-}$ animals carrying a p53 mCherry-tagged genomic rescue transgene (purple bar). *corolla* transcripts were normalized to the housekeeping gene, *rp49*. Error bars represent standard deviations from three biological replicates. $p53^{-}$ animals are significantly different from WT and p53 rescue animals (*p value < 0.0001). p53 rescue animals are not significantly different from WT (ns).

(E) *corolla* repression by p53 is Chk2 independent. *corolla* transcripts are derepressed in $p53^{-}$ animals (black bar) but effectively repressed to WT levels (blue bar) in $Chk2^{+/-}$ (dark green bar) and $Chk2^{-/-}$ (light green bar) ovaries as quantified by RT-ddPCR. *corolla* transcripts were normalized to the housekeeping gene, *rp49*. Error bars represent standard deviations from three biological replicates. $p53^{-}$ animals are significantly different from all genotypes (*p value < 0.0002). Chk2 heterozygous and $Chk2^{-}$ ovaries are not significantly different from WT (ns).

(F) *corolla* repression by p53 requires an intact p53 DNA binding motif. *corolla* transcripts are derepressed to $p53^{-}$ levels (black bar) in $p53^{+}$ animals that harbor a deletion of a p53 DNA binding motif (red triangle in A) in the *corolla* gene region (Δp53DBM, gray bar), as quantified by ovary RT-ddPCR. *corolla* transcripts were

(legend continued on next page)

transcriptional repression imposed by p53A. Collectively, these findings confirm that p53 repression operates at native targets and highlight the utility of $p53^{A\Delta5}$ as a tool for deconstructing $p53^{-}$ phenotypes and linking these to p53 repression.

DISCUSSION

Although widely studied as a stimulus-dependent inducer of transcription, mice compromised for p53 transactivation or lacking upregulated p53 effectors do not replicate cancer phenotypes seen in $p53^{-}$ animals (Brady et al., 2011; Li et al., 2012; Valente et al., 2013). These findings highlight conspicuous gaps in our understanding of p53 function and suggest that unappreciated processes may confer p53 tumor suppression (reviewed in Mello and Attardi, 2018; Boutelle and Attardi, 2021; Ho et al., 2019; and Kaiser and Attardi, 2018). We demonstrate here that repression of target genes by p53 is mediated through canonical DNA binding sites that specified p53 transactivation earlier in development (Figures 1 and 3). Furthermore, unlike gene activation, which is conditional upon stress, repression by p53 operates constitutively without a requirement for Chk2 (Figures 2 and 6). Our insights from synthetic and native *cis*-regulatory elements challenge a widely recognized model that p53 acts exclusively as a transcriptional activator (Sullivan et al., 2018). Furthermore, since the binding elements examined here match the human p53 DBM (see Figure 3A‴, Brodsky et al., 2000), we raise the possibility that p53 could suppress tumor formation by constitutively repressing genes, independent of stress and without the need for Chk2. Consistent with this, cancer susceptibilities in mice and in *Li Fraumeni* patients suggests that p53 directs tumor suppression through activities that are independent of these factors (Takai et al., 2002; Ruijs et al., 2009).

p53 genes throughout the animal kingdom generate alternatively spliced transcripts that either retain or lack the TAD (Marcel et al., 2011), raising the possibility that distinct p53 isoforms impart either repression or induction. Consistent with this, when independently targeted to $p53^{-}$ salivary glands, two isoforms (p53A or p53E) restored constitutive repression; however, in these same assays, the p53B isoform rescued induction but failed to restore repression (Figure 4). Therefore, two of the three isoforms qualify as repressors and the remaining third isoform qualifies as an activator (Table S3). Probes used to routinely map p53 occupancy generally do not distinguish between individual isoforms, and in principle, each isoform could exhibit different chromatin binding patterns, perhaps in distinct multimeric combinations. Thus, current profiles for p53 occupancy here, and in other models, may omit pivotal complexities that could be further resolved when individual isoforms are inspected (Khoury and Bourdon, 2010). Future studies with isoform-specific probes could test this possibility and explore how they instruct distinct outcomes. Nevertheless, the p53 repression we observed clearly operated through direct occupancy of canonical p53 DBMs (Figures 3 and 6) and clearly involved the formation of repressive histone marks (Figures 3 and 6), distinct from modifications associated p53 gene induction (Love et al., 2012; Kaeser and Iggo, 2004). Hence, it is possible that recruitment of unknown co-factors and/or H3K9 modifying enzymes could play a role in p53 repression studied here.

The precise mechanism of repression observed here required DNA binding, but subsequent steps have yet to be elucidated (Figures 3 and 6). Some p53 isoforms could operate directly and continuously by specifying the deposition of repressive chromatin marks and/or preventing recruitment of RNA polymerase II. Alternatively, indirect mechanisms are formally possible, and in this scenario, an induced secondary factor could, in turn, act to repress gene targets as described in previous studies (Tesfaye et al., 2021; Olivero et al., 2020; Huarte et al., 2010). However, two fundamental differences separate those findings from ours. First, insights discovered here reflect continuously repressive action in the ground state (Figures 1, 6, and 7), but in these previous examples, a challenge was imposed to "activate" p53. Second, downregulated targets in Tesfaye et al. (2021), Olivero et al. (2020), and Huarte et al. (2010) were regulated in *trans* through non-coding RNAs, but downregulated targets in this study were regulated in *cis* through repressive p53 binding sites that were functionally tested (Figures 3 and 6). Accordingly, since repression here required sites that were bound by p53 (Figures 3 and 6) and were needed for p53-mediated transactivation earlier in development (Figure 3), hypothetical intermediates would seem redundant as they would necessarily share p53-like binding properties. Results from the $p53^{A\Delta5}$ allele, which highlights residues required for repression but dispensable for transactivation (Figure 7) are also inconsistent with indirect scenarios, since an induced secondary factor should remain operational when gene activation remains intact. Thus, we favor models whereby certain p53 isoforms mediate direct repression, perhaps by recruiting distinct co-factors through residues absent from $p53^{A\Delta5}$.

Our loss-of-function studies (summarized in Table S3) linked specific p53 isoforms to distinct functions that are probably guided by tissue-specific factors and/or developmentally driven properties (Figures 5 and 6). For instance, the p53B isoform

normalized to the housekeeping gene, *rp49*. Error bars represent standard deviations from three biological replicates. WT^{CRISPR} control animals (light blue bar) that received the Cas9 and guideRNAs but were unaltered at the *corolla* locus are indistinguishable from WT animals (dark blue bar). $p53^{-}$ and Δp53DBM animals and are significantly different from WT and WT^{CRISPR} controls (*p value < 0.0001). See STAR Methods for details describing the Δp53DBM *corolla* mutation.
(G) The p53A isoform is required for *corolla* repression in ovaries, as quantified by RT-ddPCR. *corolla* transcripts were normalized to the housekeeping gene, *rp49*. Error bars represent standard deviations from three biological replicates. *corolla* RNA transcripts are significantly elevated in two independent p53A isoform mutants (dark red bars, *p value < 0.0001) when compared with two WT^{CRISPR} control animals (light blue bars). Two independent p53B (red bars) and p53E (pink bars) isoform-specific alleles are not significantly different from WT controls.
(H and I) (H–I″) Corolla repression by p53A occurs in the *Drosophila* oocyte. (H) p53 protein (red) is localized to the oocyte (yellow arrowhead) as visualized by immunostaining for an mCherry-tagged p53 rescue transgene in a $p53^{-}$ background. Nuclei are counterstained with Hoechst (blue). Scale bars, 10 μm. Note that the mCherry tag is at the C terminus and thus detects all p53 proteins (Zhang et al., 2014). (I–I″) Compared with WT animals (I) elevated Corolla (green) is seen in the oocyte (yellow arrowhead) of p53 nulls (I′) and p53A isoform knockouts. (I″) Nuclei are counterstained with Hoechst (blue). Corolla expression was unaffected in p53B or p53E isoform mutants (Figure S6). Scale bars, 10 μm.

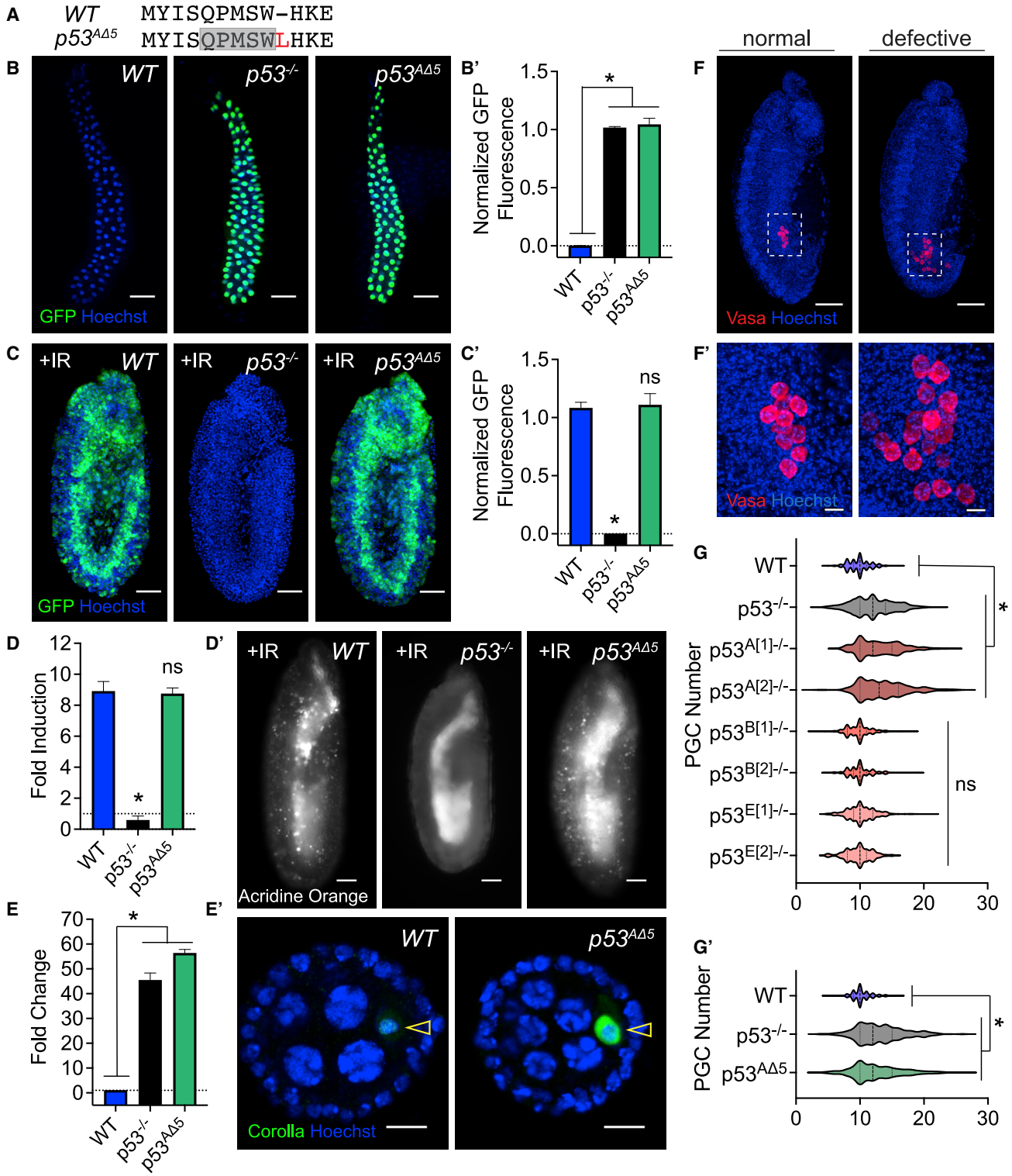

Figure 7. A unique p53A allele dissociates transcriptional activities, exposing five amino acids critical for target repression but dispensable for transactivation

(A) Diagrams the p53^{AΔ5} allele. Unique amino acids encoded by the p53A isoform are shown above, and the in-frame indel is shown below. Deleted amino acids 5–9 are shaded (gray), a Leucine insertion is indicated (red), and all other residues are unchanged (see STAR Methods).

(legend continued on next page)

was required for stress-induced transactivation in GSCs (Figure 5; Figure S5). Conversely, a single p53 isoform (p53A) coded for transrepression in salivary glands and in early oocytes (Figures 5 and 6) but, surprisingly, was also required for stimulus-dependent activity in embryos (Figure 5; Figure S7) consistent with other reports (Chakravarti et al., 2022). Although p53E had the capacity to repress in sufficiency assays (Figure 4), p53E knockouts exposed no role for this isoform in phenotypes examined here (Figure 5). Hence, the p53B isoform is a dedicated transactivator, whereas the p53A isoform is often—but not exclusively—a transrepressor, consistent with its abundance across many tissue types (Zhang et al., 2015). The direction of p53A output is probably unrelated to whether Chk2 is present, since Chk2 is clearly expressed and functional in oocytes (Abdu et al., 2002) and embryos (Lu et al., 2010). However, regarding this question, insights emerging from the $p53^{A\Delta5}$ allele are significant for several reasons (Figure 7). First, they proved that opposing transcriptional outputs coded by p53A can indeed be cleanly dissociated. Second, they highlighted five critical amino acids needed for repression but dispensable for transactivation, suggesting that pivotal co-factors might be recruited through these residues. Third, they illustrate how these strains can be used to deconstruct known $p53^{-}$ phenotypes and attribute developmental functions to p53 repression. Here, for example, using $p53^{A\Delta5}$ together with isoform-specific knockouts, we linked the repressive action of p53A to germ cell formation and to *corolla* suppression (Figure 7; Figure S7; Yamada et al., 2008; Tarayrah-Ibraheim et al., 2021). Interestingly, since *corolla* codes for a component of the synaptonemal complex (Collins et al., 2014), the misexpression of meiotic genes might contribute to developmental defects seen in $p53^{-}$ animals, and in this regard, there could be parallels to certain tumors that ectopically express germ cell-specific antigens (Whitehurst, 2014).

As a final note, our work with irradiated p53A knockout animals raised the possibility that competition among p53 isoforms could occur (Figure 5; Figures S5D′ and S5D″). For example, in irradiated WT ovaries, damage-responsive activity was highly restricted and did not appear in the somatic cells of this organ (Wylie et al., 2014) (see Figure 5). However, in irradiated p53A knockout ovaries, these same somatic cells were clearly permissive for damage-responsive induction, and importantly, this activity was completely abolished when all isoforms were missing (Figure 5). Thus, under normal circumstances, p53A prevented other isoforms from manifesting stimulus-induced activity, possibly by competing at relevant binding sites in these cells. Since fish, mouse, and human p53 counterparts code for similar isoform variants (Khoury and Bourdon, 2011; Marcel et al., 2011), tissue-specific and pleiotropic responses could similarly involve competition among repressive and activating isoforms in these settings as well (Bauer and Helfand, 2006).

Limitations of the study

Our conclusions are based on genetic and biochemical interrogations of *cis* and *trans* elements. One limitation of our study is that we lack isoform-specific p53 probes, which prevented us from inspecting occupancy by distinct p53 isoforms, perhaps in distinct multimeric combinations. Another limitation is that our p53 biosensors were quantified by fluorescence imaging (see STAR Methods), and thus, subtle differences in outputs between genotypes may not be detectable. Finally, our *in vivo* studies here are limited to *Drosophila*, and therefore, it remains to be seen whether properties of p53 repression uncovered here also extend to other systems.

(B) (B and B′) The $p53^{A\Delta5}$ allele fails to repress the p53 biosensor in salivary glands. The p53R-GFPnls biosensor is effectively repressed in WT (first column) but derepressed in $p53^{-}$ (second column) and in $p53^{A\Delta5}$ (third column) salivary glands. Glands were examined for GFP (green) and counterstained for Hoechst (blue). Patterns in (B) are quantified in (B′) where GFP fluorescence was normalized to Hoechst staining. Error bars represent standard deviations from three biological replicates. WT salivary gland biosensor activity is significantly different from $p53^{-}$ and $p53^{A\Delta5}$ animals (*p value < 0.0001). Scale bars, 100 μm.
(C) (C and C′) $p53^{A\Delta5}$ animals are normal for damage-induced transactivation. Irradiated WT (first column), $p53^{-}$ (second column), and $p53^{A\Delta5}$ (third column) embryos carrying the p53R-GFPnls biosensor transgene were examined for GFP (green) and counterstained with Hoechst (blue). Note that induced biosensor activity in WT (first column) is completely abolished in $p53^{-}$ (second column) but unaffected in $p53^{A\Delta5}$ (third column) animals. Patterns in (C) are quantified in (C′) where GFP fluorescence was normalized to Hoechst staining. Error bars represent standard deviations from three biological replicates. WT and $p53^{A\Delta5}$ embryo transactivation is not significantly different (ns). Biosensor induction in $p53^{-}$ animals is significantly different from WT and $p53^{A\Delta5}$ animals (*p value < 0.0001). Scale bars, 50 μm.
(D) (D and D′) The $p53^{A\Delta5}$ allele is normal for radiation-dependent *reaper* induction and cell death. (D) RT-ddPCR analyses show that *reaper* expression is induced in irradiated WT (blue bar) and $p53^{A\Delta5}$ (green bar) but not $p53^{-}$ (black bar) embryos. *reaper* transcripts were normalized to the housekeeping gene, *rp49*. Error bars represent standard deviations from three biological replicates. $p53^{-}$ animals are significantly different from WT and $p53^{A\Delta5}$ animals (*p value < 0.0001). $p53^{A\Delta5}$ animals are not significantly different from WT (ns). (D′) Radiation-induced cell death was examined by acridine orange staining. Note that radiation-induced cell death in WT (first column) is completely abolished in $p53^{-}$ (second column) but remains intact in $p53^{A\Delta5}$ (third column) animals. Scale bars, 50 μm.
(E) (E and E′) The $p53^{A\Delta5}$ allele is defective for *corolla* repression in ovaries. (E) RT-ddPCR analyses show that *corolla* expression is derepressed in $p53^{-}$ (black bar) and $p53^{A\Delta5}$ (green bar) ovaries (black bar) when compared with WT animals (blue bar). *corolla* transcripts were normalized to the housekeeping gene, *rp49*. Error bars represent standard deviations from three biological replicates. $p53^{-}$ and $p53^{A\Delta5}$ animals are significantly different WT (*p value < 0.0001). (E′) Immunodetection experiments show that the $p53^{A\Delta5}$ allele is defective for Corolla repression in the early oocyte. Elevated Corolla protein expression (green) in the oocyte (yellow arrowhead) in $p53^{A\Delta5}$ (second column) compared with a WT animal (first column). Nuclei are counterstained with Hoechst (blue). Scale bars, 20 μm.
(F and G) (F–G′) Primordial germ cell (PGC) defects seen in $p53^{-}$ animals replicate in p53A knockouts and $p53^{A\Delta5}$ alleles. (F) Stage 14 embryos were immunostained for Vasa (red) and counterstained with Hoechst (blue) to assess PGC number. Panels in (F) and (F′) show examples of normal (first column) and defective (second column) PGC numbers in $p53^{-}$ animals as previously reported (Tarayrah-Ibraheim et al., 2021; Yamada et al., 2008). Magnified images of PGCs in (F, white box) are provided in (F′) to better appreciate the PGC defect. Scale bars: 50 μm in (F) and 10 μm in (F′). PGC numbers where quantified in (G) and (G′). (G) PGC numbers were quantified and significantly elevated in $p53^{-}$ (gray bar) and two independent p53A knockouts (dark red bars, *p value < 0.0001) when compared with two WT control animals (blue bars). Two independent p53B (red bars) and p53E (pink bars) isoform-specific knockouts are not significantly different from WT controls. 96–204 biological samples were quantified per genotype in (G). (G′) PGC numbers were quantified and significantly elevated in $p53^{-}$ (gray bar, *p value < 0.0001) and $p53^{A\Delta5}$ animals (green bars bar, *p value < 0.0001) when compared with two WT control animals (blue bar). Note that all animals in (B)–(G′) were homozygous for the designated allele. 175–225 biological samples were quantified per genotype in (G′).

STAR★METHODS

Detailed methods are provided in the online version of this paper and include the following:

- KEY RESOURCES TABLE
- RESOURCE AVAILABILITY
  - Lead contact
  - Materials availability
  - Data and code availability
- EXPERIMENTAL MODEL AND SUBJECT DETAILS
  - Construction of the p53 biosensors
  - Fly stocks and genetics
- METHOD DETAILS
  - Irradiation studies
  - Immunostaining of fly tissue
  - Acridine orange staining
  - Microscopy and image quantification
  - CRISPR/Cas9 genome editing
  - RNAi and addback constructs
  - Ovary chromatin immunoprecipitation ddPCR
  - CUT&RUN
  - CUT&RUN data analysis
  - RT-PCR
- QUANTIFICATION AND STATISTICAL ANALYSIS

SUPPLEMENTAL INFORMATION

Supplemental information can be found online at https://doi.org/10.1016/j.devcel.2022.06.015.

ACKNOWLEDGMENTS

This work was supported by grants to A.W. (National Institutes of Health [NIH] 5T32CA124334), S.D. (Cancer Prevention and Research Institute of Texas [CPRIT] training grant RP160157), and J.M.A. (NIH R01GM115682, NIH R01CA222579, CPRIT RP170086 and support from the SCCC Translational Pilot Program). We thank the McDermott Center Next-Generation Core Facility at University of Texas Southwestern and gratefully acknowledge the assistance of the University of Texas Southwestern Live-Cell Imaging Facility, a shared resource of the Harold C. Simmons Cancer Center, supported in part by National Cancer Institute Cancer Center Support Grant P30 CA142543. We thank the UTSW BioHPC, the UTSW preclinical radiation core facility, and the Texas Advanced Computing Center at the University of Texas at Austin (TACC) for providing HPC resources used in the analysis of next-generation sequencing data sets. We are grateful to Drs. Calvi, Schupbach, and Hawley for strains and reagents.

AUTHOR CONTRIBUTIONS

A.W., A.E.J., S.D., and W-J.L. contributed to this manuscript in conception and design, acquisition of data, analysis and interpretation of data, and drafting or revising the article. J.M.A. contributed to this manuscript in conception and design, analysis and interpretation of data, and drafting or revising the article.

DECLARATION OF INTERESTS

The authors declare no competing interests.

Received: August 9, 2021
Revised: February 15, 2022
Accepted: June 15, 2022
Published: July 11, 2022

REFERENCES

Abdu, U., Brodsky, M., and Schüpbach, T. (2002). Activation of a meiotic checkpoint during Drosophila oogenesis regulates the translation of Gurken through Chk2/Mnk. Curr. Biol. *12*, 1645–1651.

Ahmed, K. (2018). CUT&RUN with Drosophila tissues. https://www.protocols.io/view/cut-run-with-drosophila-tissues-14egnx28pl5d/v1.

Ahn, J., Urist, M., and Prives, C. (2004). The Chk2 protein kinase. DNA Repair (Amst) *3*, 1039–1047.

Akdemir, F., Christich, A., Sogame, N., Chapo, J., and Abrams, J.M. (2007). p53 directs focused genomic responses in Drosophila. Oncogene *26*, 5184–5193.

Barolo, S., Carver, L.A., and Posakony, J.W. (2000). GFP and beta-galactosidase transformation vectors for promoter/enhancer analysis in Drosophila. BioTechniques *29*, 726, 728–730, 732.

Bauer, J.H., and Helfand, S.L. (2006). New tricks of an old molecule: lifespan regulation by p53. Aging Cell *5*, 437–440.

Beckerman, R., and Prives, C. (2010). Transcriptional regulation by p53. Cold Spring Harb. Perspect. Biol. *2*, a000935.

Boutelle, A.M., and Attardi, L.D. (2021). p53 and tumor suppression: it takes a network. Trends Cell Biol. *31*, 298–310.

Brady, C.A., Jiang, D., Mello, S.S., Johnson, T.M., Jarvis, L.A., Kozak, M.M., Kenzelmann Broz, D.K., Basak, S., Park, E.J., Mclaughlin, M.E., et al. (2011). Distinct p53 transcriptional programs dictate acute DNA-damage responses and tumor suppression. Cell *145*, 571–583.

Brodsky, M.H., Nordstrom, W., Tsang, G., Kwan, E., Rubin, G.M., and Abrams, J.M. (2000). Drosophila p53 binds a damage response element at the reaper locus. Cell *101*, 103–113.

Chakravarti, A., Thirimanne, H.N., Brown, S., and Calvi, B.R. (2022). Drosophila p53 isoforms have overlapping and distinct functions in germline genome integrity and oocyte quality control. eLife *11*, e61389.

Chanas, G., Lavrov, S., Iral, F., Cavalli, G., and Maschat, F. (2004). Engrailed and polyhomeotic maintain posterior cell identity through cubitus-interruptus regulation. Dev. Biol. *272*, 522–535.

Chaudhary, R., and Lal, A. (2017). Long noncoding RNAs in the p53 network. Wiley Interdiscip. Rev. RNA *8*, e1410.

Collins, K.A., Unruh, J.R., Slaughter, B.D., Yu, Z., Lake, C.M., Nielsen, R.J., Box, K.S., Miller, D.E., Blumenstiel, J.P., Perera, A.G., et al. (2014). Corolla is a novel protein that contributes to the architecture of the synaptonemal complex of Drosophila. Genetics *198*, 219–228.

Denton, D., and Kumar, S. (2015). Using the vital dye acridine orange to detect dying cells in Drosophila. Cold Spring Harb. Protoc. *2015*, 572–575.

Dobin, A., Davis, C.A., Schlesinger, F., Drenkow, J., Zaleski, C., Jha, S., Batut, P., Chaisson, M., and Gingeras, T.R. (2013). STAR: ultrafast universal RNA-seq aligner. Bioinformatics *29*, 15–21.

El-Deiry, W.S., Kern, S.E., Pietenpol, J.A., Kinzler, K.W., and Vogelstein, B. (1992). Definition of a consensus binding site for p53. Nat. Genet. *1*, 45–49.

Feng, Z., Zhang, C., Wu, R., and Hu, W. (2011). Tumor suppressor p53 meets microRNAs. J. Mol. Cell Biol. *3*, 44–50.

Fischer, M. (2017). Census and evaluation of p53 target genes. Oncogene *36*, 3943–3956.

Fischer, M., Quaas, M., Steiner, L., and Engeland, K. (2016). The p53-p21-DREAM-CDE/CHR pathway regulates G2/M cell cycle genes. Nucleic Acids Res. *44*, 164–174.

Gibson, D.G., Young, L., Chuang, R.Y., Venter, J.C., Hutchison, C.A., 3rd, and Smith, H.O. (2009). Enzymatic assembly of DNA molecules up to several hundred kilobases. Nat. Methods *6*, 343–345.

Gratz, S.J., Ukken, F.P., Rubinstein, C.D., Thiede, G., Donohue, L.K., Cummings, A.M., and O'Connor-Giles, K.M. (2014). Highly specific and efficient CRISPR/Cas9-catalyzed homology-directed repair in Drosophila. Genetics *196*, 961–971.

Gratz, S.J., Wildonger, J., Harrison, M.M., and O'Connor-Giles, K.M. (2013). CRISPR/Cas9-mediated genome engineering and the promise of designer flies on demand. Fly (Austin) *7*, 249–255.

Groth, A.C., Fish, M., Nusse, R., and Calos, M.P. (2004). Construction of transgenic Drosophila by using the site-specific integrase from phage phiC31. Genetics *166*, 1775–1782.

Hirao, A., Kong, Y.Y., Matsuoka, S., Wakeham, A., Ruland, J., Yoshida, H., Liu, D., Elledge, S.J., and Mak, T.W. (2000). DNA damage-induced activation of p53 by the checkpoint kinase Chk2. Science *287*, 1824–1827.

Ho, T., Tan, B.X., and Lane, D. (2019). How the other half lives: what p53 does when it is not being a transcription factor. Int. J. Mol. Sci. *21*, 13.

Huarte, M., Guttman, M., Feldser, D., Garber, M., Koziol, M.J., Kenzelmann-Broz, D., Khalil, A.M., Zuk, O., Amit, I., Rabani, M., et al. (2010). A large intergenic noncoding RNA induced by p53 mediates global gene repression in the p53 response. Cell *142*, 409–419.

Kaeser, M.D., and Iggo, R.D. (2004). Promoter-specific p53-dependent histone acetylation following DNA damage. Oncogene *23*, 4007–4013.

Kaiser, A.M., and Attardi, L.D. (2018). Deconstructing networks of p53-mediated tumor suppression in vivo. Cell Death Differ. *25*, 93–103.

Khoury, M.P., and Bourdon, J.C. (2010). The isoforms of the p53 protein. Cold Spring Harb. Perspect. Biol. *2*, a000927.

Khoury, M.P., and Bourdon, J.C. (2011). p53 isoforms: an intracellular microprocessor? Genes Cancer *2*, 453–465.

Kurtz, P., Jones, A.E., Tiwari, B., Link, N., Wylie, A., Tracy, C., Krämer, H., and Abrams, J.M. (2019a). Drosophila p53 directs nonapoptotic programs in postmitotic tissue. Mol. Biol. Cell *30*, 1339–1351.

Langmead, B., and Salzberg, S.L. (2012). Fast gapped-read alignment with Bowtie 2. Nat. Methods *9*, 357–359.

Li, T., Kon, N., Jiang, L., Tan, M., Ludwig, T., Zhao, Y., Baer, R., and Gu, W. (2012). Tumor suppression in the absence of p53-mediated cell-cycle arrest, apoptosis, and senescence. Cell *149*, 1269–1283.

Link, N., Kurtz, P., O'Neal, M., Garcia-Hughes, G., and Abrams, J.M. (2013). A p53 enhancer region regulates target genes through chromatin conformations in cis and in trans. Genes Dev. *27*, 2433–2438.

Love, I.M., Sekaric, P., Shi, D., Grossman, S.R., and Androphy, E.J. (2012). The histone acetyltransferase PCAF regulates p21 transcription through stress-induced acetylation of histone H3. Cell Cycle *11*, 2458–2466.

Lu, W.J., Chapo, J., Roig, I., and Abrams, J.M. (2010). Meiotic recombination provokes functional activation of the p53 regulatory network. Science *328*, 1278–1281.

Marcel, V., Dichtel-Danjoy, M.L., Sagne, C., Hafsi, H., Ma, D., Ortiz-Cuaran, S., Olivier, M., Hall, J., Mollereau, B., Hainaut, P., et al. (2011). Biological functions of p53 isoforms through evolution: lessons from animal and cellular models. Cell Death Differ. *18*, 1815–1824.

Mello, S.S., and Attardi, L.D. (2018). Deciphering p53 signaling in tumor suppression. Curr. Opin. Cell Biol. *51*, 65–72.

Müller, H.A. (2008). Immunolabeling of embryos. Methods Mol. Biol. *420*, 207–218.

Nègre, N., Hennetin, J., Sun, L.V., Lavrov, S., Bellis, M., White, K.P., and Cavalli, G. (2006). Chromosomal distribution of PcG proteins during Drosophila development. PLoS Biol. *4*, e170.

Ni, J.Q., Zhou, R., Czech, B., Liu, L.P., Holderbaum, L., Yang-Zhou, D., Shim, H.S., Tao, R., Handler, D., Karpowicz, P., et al. (2011). A genome-scale shRNA resource for transgenic RNAi in Drosophila. Nat. Methods *8*, 405–407.

Olivero, C.E., Martínez-Terroba, E., Zimmer, J., Liao, C., Tesfaye, E., Hooshdaran, N., Schofield, J.A., Bendor, J., Fang, D., Simon, M.D., et al. (2020). p53 activates the long noncoding RNA Pvt1b to inhibit Myc and suppress tumorigenesis. Mol. Cell *77*, 761–774.e8.

Peters, M., Deluca, C., Hirao, A., Stambolic, V., Potter, J., Zhou, L., Liepa, J., Snow, B., Arya, S., Wong, J., et al. (2002). Chk2 regulates irradiation-induced, p53-mediated apoptosis in *Drosophila*. Proc. Natl. Acad. Sci. USA *99*, 11305–11310.

Ramírez, F., Ryan, D.P., Grüning, B., Bhardwaj, V., Kilpert, F., Richter, A.S., Heyne, S., Dündar, F., and Manke, T. (2016). deepTools2: a next generation web server for deep-sequencing data analysis. Nucleic Acids Res. *44*, W160–W165.

Robin, J.D., Ludlow, A.T., Batten, K., Magdinier, F., Stadler, G., Wagner, K.R., Shay, J.W., and Wright, W.E. (2014). Telomere position effect: regulation of gene expression with progressive telomere shortening over long distances. Genes Dev. *28*, 2464–2476.

Ruijs, M.W., Broeks, A., Menko, F.H., Ausems, M.G., Wagner, A., Oldenburg, R., Meijers-Heijboer, H., Van'T Veer, L.J., and Verhoef, S. (2009). The contribution of CHEK2 to the TP53-negative Li-Fraumeni phenotype. Hered. Cancer Clin. Pract. *7*, 4.

Schmieder, R., and Edwards, R. (2011). Quality control and preprocessing of metagenomic datasets. Bioinformatics *27*, 863–864.

Skene, P.J., and Henikoff, S. (2017). An efficient targeted nuclease strategy for high-resolution mapping of DNA binding sites. eLife *6*, e21856.

Sogame, N., Kim, M., and Abrams, J.M. (2003). Drosophila p53 preserves genomic stability by regulating cell death. Proc. Natl. Acad. Sci. USA *100*, 4696–4701.

Soussi, T. (2007). p53 alterations in human cancer: more questions than answers. Oncogene *26*, 2145–2156.

Soussi, T., and Wiman, K.G. (2015). TP53: an oncogene in disguise. Cell Death Differ. *22*, 1239–1249.

Sullivan, K.D., Galbraith, M.D., Andrysik, Z., and Espinosa, J.M. (2018). Mechanisms of transcriptional regulation by p53. Cell Death Differ. *25*, 133–143.

Takai, H., Naka, K., Okada, Y., Watanabe, M., Harada, N., Saito, S., Anderson, C.W., Appella, E., Nakanishi, M., Suzuki, H., et al. (2002). Chk2-deficient mice exhibit radioresistance and defective p53-mediated transcription. EMBO J. *21*, 5195–5205.

Tanikawa, C., Zhang, Y.Z., Yamamoto, R., Tsuda, Y., Tanaka, M., Funauchi, Y., Mori, J., Imoto, S., Yamaguchi, R., Nakamura, Y., et al. (2017). The transcriptional landscape of p53 signalling pathway. EBiomedicine *20*, 109–119.

Tarayrah-Ibraheim, L., Maurice, E.C., Hadary, G., Ben-Hur, S., Kolpakova, A., Braun, T., Peleg, Y., Yacobi-Sharon, K., and Arama, E. (2021). DNase II mediates a parthanatos-like developmental cell death pathway in Drosophila primordial germ cells. Nat. Commun. *12*, 2285.

Tesfaye, E., Martinez-Terroba, E., Bendor, J., Winkler, L., Olivero, C., Chen, K., Feldser, D.M., Zamudio, J.R., and Dimitrova, N. (2021). The p53 transcriptional response across tumor types reveals core and senescence-specific signatures modulated by long noncoding RNAs. Proc. Natl. Acad. Sci. USA *118*. e2025539118.

Valente, L.J., Gray, D.H., Michalak, E.M., Pinon-Hofbauer, J., Egle, A., Scott, C.L., Janic, A., and Strasser, A. (2013). p53 efficiently suppresses tumor development in the complete absence of its cell-cycle inhibitory and proapoptotic effectors p21, puma, and noxa. Cell Rep. *3*, 1339–1345.

Vousden, K.H., and Lane, D.P. (2007). p53 in health and disease. Nat. Rev. Mol. Cell Biol. *8*, 275–283.

Wang, B., Xiao, Z., Ko, H.L., and Ren, E.C. (2010). The p53 response element and transcriptional repression. Cell Cycle *9*, 870–879.

Wang, Y., Schwedes, J.F., Parks, D., Mann, K., and Tegtmeyer, P. (1995). Interaction of p53 with its consensus DNA-binding site. Mol. Cell. Biol. *15*, 2157–2165.

Whitehurst, A.W. (2014). Cause and consequence of cancer/testis antigen activation in cancer. Annu. Rev. Pharmacol. Toxicol. *54*, 251–272.

Wylie, A., Jones, A.E., D'Brot, A., Lu, W.J., Kurtz, P., Moran, J.V., Rakheja, D., Chen, K.S., Hammer, R.E., Comerford, S.A., et al. (2016). p53 genes function to restrain mobile elements. Genes Dev. *30*, 64–77.

Wylie, A., Lu, W.J., D'Brot, A., Buszczak, M., and Abrams, J.M. (2014). p53 activity is selectively licensed in the Drosophila stem cell compartment. eLife *3*, e01530.

Xie, H.B., and Golic, K.G. (2004). Gene deletions by ends-in targeting in *Drosophila melanogaster*. Genetics *168*, 1477–1489.

Yamada, Y., Davis, K.D., and Coffman, C.R. (2008). Programmed cell death of primordial germ cells in Drosophila is regulated by p53 and the Outsiders monocarboxylate transporter. Development *135*, 207–216.

Zhang, B., Mehrotra, S., Ng, W.L., and Calvi, B.R. (2014). Low levels of p53 protein and chromatin silencing of p53 target genes repress apoptosis in drosophila endocycling cells. PLoS Genet. *10*, e1004581.

Zhang, B., Rotelli, M., Dixon, M., and Calvi, B.R. (2015). The function of Drosophila p53 isoforms in apoptosis. Cell Death Differ. *22*, 2058–2067.

STAR★METHODS

KEY RESOURCES TABLE

REAGENT or RESOURCE	SOURCE	IDENTIFIER
Antibodies		
α-rabGFP	ThermoFisher Scientific	Cat # A11122; RRID: AB_221569
α-rabDsRed)	TaKaRa	Cat # Living Colors® DsRed, 632496; RRID: AB_10013483
α-mouseProspero	DSHB	MR1A; RRID: AB_528440
α-mouseCrumbs	DSHB	Cq4; RRID: AB_528181
α-mouse-HTS	DSHB	1B1; RRID: AB_528070
α-rabCorolla	Scott Hawley, Stowers Institute	(Collins et al., 2014)
Alexa-rab488,	Invitrogen	Cat# A32731; RRID: AB_2633280
Alexa-rab568	Invitrogen	Cat#A11011; RRID: AB_143157
Alexa-mouse488	Invitrogen	Cat#A21200; RRID: AB_2535786
Alexa-mouse568	Invitrogen	Cat#A11004; RRID: AB_2534072
H3K9m3	Abcam	Cat#ab8898; RRID: AB_306848
H3K4m3 Active Motif	ThermoFisher Scientific	39159
Experimental models: Organisms/strains		
p53[K1]-/-	Bloomington Drosophila Stock Center (Xie and Golic, 2004)	BDSC6815
p53[NS]-/-	Bloomington Drosophila Stock Center (Sogame et al., 2003)	BDSC 23283
Ubiquitous-Cre	Bloomington Drosophila Stock Center	BDSC 851
sg-p53RNAi	This Study	N/A
sg-Chk2RNAi	This Study	N/A
p53gRescue;p53[K1]-/-	John Abrams, UT Southwestern Medical Center	(Wylie et al., 2014)
p53gRescue-mCherry;p53[K1]-/-	Brian Calvi, Indiana University Bloomington	(Zhang et al., 2015)
mnk[p6]-/- (Chk2-/-)	Gertrud M. Schüpbach, Princeton University	(Abdu et al., 2002)
p53R-GFPnls	John Abrams, UT Southwestern Medical Center	(Lu et al., 2010)
p53R-GFPcyt	John Abrams, UT Southwestern Medical Center	(Lu et al., 2010)
p53R-GFP-attBnls	This Study	N/A
p53R-GFPnlsΔDBM(1)	This Study	N/A
p53R-GFPnlsΔDBM(2)	This Study	N/A
p53R-GFPnlsΔDBM(3)	This Study	N/A
p53R-GFPnlsΔDBM(4)	This Study	N/A
p53R-GFPnlsΔDBM(5)	This Study	N/A
p53R-GFPattBnlsΔDBM	This Study	N/A
corollaΔDBM	This Study	N/A
p53A[1]-/-	This Study	N/A
p53A[2]-/-	This Study	N/A
p53AΔ5	This Study	N/A
p53B[1]-/-	This Study	N/A
p53B[2]-/-	This Study	N/A
p53E[1]-/-	This Study	N/A
p53E[2]-/-	This Study	N/A
sg-p53A-mCh; p53[K1]-/- (addback)	This Study	N/A
sg-p53B-mCh; p53[K1]-/- (addback)	This Study	N/A
sg-p53E-mCh; p53[K1]-/- (addback)	This Study	N/A
sg-mCh; p53[K1]-/- (addback)	This Study	N/A

(*Continued on next page*)

Continued

REAGENT or RESOURCE	SOURCE	IDENTIFIER
Chemicals and commercial kits		
Acridine Orange	Sigma Aldrich	A6014
Hoechst 33342	Invitrogen	H3570
VECTASHIELD antifade mounting medium	Vector Laboratories	H-1000
16% formaldehyde Solution, methanol free	ThermoScientific	28908
Heptane	Sigma Aldrich	494526-1L
Trizol	Life Technologies	15596026
TURBO DNA-free kit	Invitrogen	AM1907
iScript™ Reverse Transcription Supermix	BioRad	1708841
QX200 EvaGreen ddPCR supermix	BioRad	1864034
Droplet Generation Oil for EvaGreen	BioRad	1864005
Droplet Reader Oil	BioRad	1863004
Protease Inhibitors	Roche	11836170001
Concavalin A Beads	Bangs Laboratories	BP531
Digitonin	ThermoFisher Scientific	BN2006
Protein A MNase	Stephen Henikoff, Fred Hutchinson Cancer Center	(Skene and Henikoff, 2017)
the NEXTFLEX RAPID DNA-seq Kit 2.0	Bioo NOVA	5188-12
GoTaq Green Master mix	(Promega	M7123
BbsI	New England Biolabs	R0539L
BstX1	New England Biolabs	R0113L
FatI	New England Biolabs	R0650L
Deposited data		
Cut&Run sequencing data have been deposited at GEO	https://www.ncbi.nlm.nih.gov/geo/	GSE196734
Recombinant DNA		
pH-Stinger	DGRC	1018
pU6-Bbs1-chiRNA	Addgene (Gratz et al., 2013)	45946
pDsRed-attp	Addgene	51019
Software and algorithms		
Adobe Photoshop	Adobe Systems	Adobe Systems
Adobe Illustrator	Adobe Systems	Adobe Systems
ImageJ	NIH	NIH
Prism	GraphPad Software, Inc	GraphPad Software, Inc

RESOURCE AVAILABILITY

Lead contact

Further information and requests for resources and reagents should be directed to and will be fulfilled by the lead contact, John Abrams (john.abrams@utsouthwestern.edu).

Materials availability

Fly strains generated in this study are available through the lead author, John Abrams (john.abrams@utsouthwestern.edu).

Data and code availability

Cut&Run sequencing data have been deposited at GEO and are publicly available as of the date of publication. Accession numbers are listed in the key resources table. Microscopy data reported in this paper will be shared by the lead contact upon request. Any additional information required to reanalyze the data reported in this paper is available from the lead contact upon request.

EXPERIMENTAL MODEL AND SUBJECT DETAILS

Construction of the p53 biosensors

We previously uncovered a 150bp minimal p53 radiation responsive element in the reaper enhancer (Brodsky et al., 2000) and placed this upstream of GFP (p53R-GFP) (Lu et al., 2010). This 150bp sequence contains a bioinformatically predicted p53 binding site (p53DBM, two adjacent 10mers, no spacing) and this sequence is identical to the human consensus site but diverges at the two most terminal nucleotides (see Figure 3A‴) (Brodsky et al., 2000). Transgenic fly strains are made with two reporter constructs, one contains a nuclear localization signal for GFP (p53R-GFPnls) and the other one does not (p53R-GFPcyt) (Figures 1A and 1B). These biosensors require wild-type p53 and are effective readouts for p53 function (Lu et al., 2010).

To adapt the p53 biosensor for phiC31 recombination system (Groth et al., 2004), an attB sequence was cloned into the p53 biosensor plasmid (p53R-GFP-attBnls; Table S1; Figures S1N–S1N‴, S2E–S2E″, and S3A–S3B′). The p53DBM deletion within the biosensor was generated using Gibson assembly (Gibson et al., 2009). All plasmid constructs were injected into Bloomington #9752 y[1] w[1118]; PBacy[+]-attP-3BVK00037 flies in order to place all p53 biosensor alteration into the same genomic location. These biosensor flies were used in Table S1 and Figures S1N–S1N‴, S2E–S2E″, and S3A–S3B′).

Fly stocks and genetics

All fly stocks were maintained at 22-25°C on standard food media. We used two *Drosophila* p53 (Dp53) genomic rescue strains previously described in Wylie et al. (2016), Zhang et al. (2015), and Wylie et al. (2014). The untagged Dp53 rescue strain was used in Figures 1A–1C and the $p53^{mCh}$ flies were used for all other rescue experiments. Note that the untagged Dp53 genomic rescue strain ($p53^{gRes}$;$p53^{-}$) is expressed at physiologic levels (Wylie et al., 2014). We obtained mCherry-tagged p53 Rescue strains from B. Calvi (Indiana University, Bloomington, IN, USA). We obtained Chk2 mutant (mnk[p6]) from T. Schupbach (Princeton University, Princeton, NJ, USA). We obtained nanos>Cas9 flies from M. Buszczak (UT Southwestern, Dallas, TX, USA). To examine effects of p53 loss on the p53 biosensors, two p53 null alleles were used: 5A-1-4 (k1) and 238H (ns).

METHOD DETAILS

Irradiation studies

For p53 biosensor induction assays, *Drosophila* embryos were collected for 1hr on standard juice media, aged for 4hrs, exposed to 40Gy of ionizing radiation using a Cs-137 Mark 1-68A irradiator (J.L.Shepherd & Associates, San Ferando, CA, USA) and recovered for 3-4hrs. Embryos were then fixed and processed for immunostaining (see below).

For p53 biosensor induction assays on *Drosophila* 3rd instar salivary glands, 3rd instar larvae were exposed to 40Gy of ionizing radiation using a Cs-137 Mark 1-68A irradiator (J.L.Shepherd & Associates, San Ferando, CA, USA). Salivary glands were dissected in PBS and imaged live at 45min, 1.5hr, 3hr and 4hr post-irradiation. Unirradiated controls were imaged for comparison. The irradiation time course could not be carried out longer since 3rd instar larvae pupated past 4 hours of irradiation.

For p53 irradiation studies on ovaries, fattened female flies were exposed to 40Gy of ionizing radiation using a Cs-137 Mark 1-68A irradiator and recovered for 24hrs. Ovaries were then fixed and processed for immunostaining.

For *reaper* induction or Acridine Orange staining, embryos were collected for 1hr on standard juice media, aged for 3hrs, exposed to 40Gy of ionizing radiation using a Cs-137 Mark 1-68A irradiator (J.L.Shepherd & Associates, San Ferando, CA, USA) and recovered for 1.5hrs. Embryos were then processed for RNA extraction or Acridine Orange staining (see below).

Immunostaining of fly tissue

Embryos were fixed according to established protocols (Müller, 2008). Embryos were stored at -20 C in methanol for at least 24hrs and rehydrated in PBS +0.1%Triton (PBST) before starting immunostaining protocol. 3rd instar salivary glands were fixed in 4% paraformaldehyde (Fisher Scientific) diluted PBST with equal volumes of heptane for 75 minutes under agitation before proceeding with immunostaining protocols for ovary IHC. Ovary IHC was performed as outlined in (Wylie et al., 2014). The following primary antibodies were used: α-rabGFP (ThermoFisher Scientific, A11122), α-rabDsRed for visualizing mCherry p53 Rescue (TaKaRa, Living Colors® DsRed, 632496), α-mouseProspero (DSHB, MR1A), α-mouseCrumbs (DSHB, Cq4), α-mouse-HTS (DSHB, 1B1). The Corolla antibody was a kind gift from Scott Hawley (Collins et al., 2014). For fluorescence visualization, the following secondary antibodies were used: Alexa-rab488, Alexa-rab568, Alexa-mouse488, Alexa-mouse568 (Invitrogen, Grand Island, NY, USA). For nuclei visualization 0.1μg/mL of Hoechst (Invitrogen) for DNA staining was added after secondary antibody incubation. Tissue was mounted in VECTASHIELD (Vector Laboratories) for microscopy imaging.

Acridine orange staining

Acridine orange staining in irradiated embryos was performed according to published protocols (Denton and Kumar, 2015). Briefly, embryos were dechorionated in 50% bleach. Embryos were transferred to a tube containing equal volumes of heptane and 5ug/mL Acridine orange in PBS and shaken vigorously for 5 minutes. Embryos were then placed on a microscope slide and imaged under halocarbon oil.

Microscopy and image quantification

Salivary gland images were taken with a Multiphoton Zeiss LSM780 upright confocal microscope using a 10× objective lens with Zeiss Zen software. Fluorescent images of whole-mount larvae or multiple salivary glands were taken on the Zeiss SteREO Discovery V.12 microscope using the 1.50× lens with AxioVision software. Embryo images were taken with a Multiphoton Zeiss LSM780 upright confocal microscope using a 20× objective lens with Zeiss Zen software. Ovary images were taken with a Multiphoton Zeiss LSM780 upright confocal microscope using a 40W× objective lens with Zeiss Zen software. Antibody staining image comparisons between wild-type, $p53^{-}$, and all other indicated genotypes were done with the same laser image intensities and master gain settings. Z-stacks were taken at 0.5-μm sections. Z-stacks of images were projected using ImageJ software (National Institutes of Health). The Z-stacks were projected using the maximum fluorescence intensity and the total area of the GFP signal was normalized to Hoechst signal (normalized Fluorescence intensity) of each respective salivary gland or embryo. Ratios were graphed on Prism software and statistical analysis was performed using one-way ANOVA. Figures were prepared using Adobe Photoshop and Illustrator CS2 (Adobe Systems).

CRISPR/Cas9 genome editing

All single-guide RNAs (sgRNAs) were cloned in pU6-Bbs1-chiRNA vector as previously described (Gratz et al., 2013). Primers used for sgRNA cloning are listed in Table S6. For CRISPR/Cas9 mediated deletions of the biosensor p53DBM, the p53R-GFPnls flies were crossed to a nanos>Cas9 fly stock to generate: p53R-GFPnls;nanosCas9 fly. These flies were injected with 4 guide RNA expressing plasmids by Rainbow Transgenic Flies. Individual F0 flies were crossed to Yw wild type strains and F1 offspring were screened for biosensor activity in salivary glands. Stable stocks were generated and Sanger sequencing was performed through the biosensor locus.

For generating p53 isoform specific alleles, 3-4 sgRNAs were injected into nanosCas9 expressing flies to target the unique exon encoded by each isoform. Individual F1 offspring were PCR screened with GoTaq Green Master mix (Promega), followed by restriction digest for 'Failure to Cut' as a putative lesion in the unique exon (p53B: BbsI (NEB), p53A: BstXI (NEB), p53E: FatI (NEB). Sanger sequencing was subsequently performed through the entire p53 gene locus.

For targeting the p53 DBM in the *corolla* gene locus, one sgRNA with a pDsRed-attp homology donor plasmid containing the p53DBM deletion were co-injected into nanosCas9 expressing flies. pDsRed-attP was a gift from Melissa Harrison & Kate O'Connor-Giles & Jill Wildonger (Addgene plasmid # 51019; http://n2t.net/addgene:51019; RRID:Addgene_51019). Homology donor cloning was performed as described in Gratz et al. (2014). F1 flies were screened for dsRed positive eyes and were sequenced for deletion of the *corolla* p53 DBM. The dsRed marker was removed by crossing to a ubiquitously expressing Cre fly (Bloomington # 851 y[1] w[67c23] Py[+mDint2]=Crey1b; D[*]/TM3, Sb[1].

RNAi and addback constructs

The biosensor backbone (pH-Stinger) drives expression in salivary glands (Barolo et al., 2000). Therefore, we modified pH-Stinger, adding an attB sequence to produce the pH-Stinger-attB. Next, we replaced GFP with the Walium20 sequence for high expression of hairpin inserts between the EcoRI and HpaI restriction site (Ni et al., 2011). p53 and Chk2 shRNAs were cloned as outlined by DRSC/TRiP Functional Genomics Resources & DRSC-BTRR (https://fgr.hms.harvard.edu/cloning-and-sequencing). Oligos for p53 shRNA are listed in Table S6. Note that RNAi occurs in late embryonic salivary glands and persists until the third instar larval stage where we examine biosensor activity (about 4 days). For addback constructs we replaced the GFP in pH-Stinger-attB with cDNA sequences of each *Drosophila* p53 isoform. These cDNAs were also N-terminal mCherry tagged so expression could be assessed. Transgenic flies were generated by phiC injection into Bloomington #9752 PBacy[+]-attP-3BVK00037.

Ovary chromatin immunoprecipitation ddPCR

We employed a previously published Chromatin Immunoprecipitation protocol (Chanas et al., 2004; Nègre et al., 2006; Kurtz et al., 2019a, 2019b) with adaptations. In brief, ovaries were dissected from age matched fattened females and fixed intact in 1% Formaldehyde in PBS containing protease inhibitors (Roche 11836170001). Glycine was added (125mM final) to quench fixation, ovaries were incubated on ice for 5 minutes, washed three times with PBS containing protease inhibitors, aspirated and flash frozen. Ovaries were stored at -80C until 300 pairs of ovaries had been dissected for each genotype. Ovaries were then thawed on ice, resuspended in lysis buffer (140 mM NaCl, 15 mM HEPES, pH 7.6, 1 mM EDTA, 0.5 mM EGTA [ethylene glycol tetraacetic acid], 0.1% sodium deoxycholate, 1% Triton X-100, 0.1% SDS, 0.5% N-lauroylsarcosine, and protease inhibitors) and homogenized. Chromatin was sheared to an average of 300-700bp with a Covaris Sonicator (5 minutes, 200 cpb, intensity 5). Samples were extracted for an additional 10 minutes while rotating at 4C, before being spun down at 13.2krpm for 10 minutes and 4C. Supernatant was transferred to a clean tube and the pellet was resuspended in 150uL of lysis buffer and extracted again for 10 minutes at 4C. Insoluble components were removed by centrifugation (13.2krpm, 10 minutes, 4C), and supernatants were pooled. Combined supernatants were centrifuged an additional five times at 13.2krpm for 10 minutes per spin at 4C to remove lipid and other insoluble components. Following centrifugation, supernatant was transferred to a lo-bind Eppendorf tube and the volume was adjusted to 1.5mL with addition of lysis buffer containing protease inhibitors. Input (10%) was retained, and the remaining material was used for mCh-p53 ChIP (dsRed Takara 632496), matched IgG control (Diagenode C15410206) and histone ChIPs (H3K9m3 Abcam ab8898, H3K4m3 Active Motif 39159). For all ChIPs, 2 ug of antibody was incubated with chromatin overnight at 4C on a nutator. Samples were then spun at 13.2krpm for 10min at 4C and supernatant was transferred to a clean tube containing 3x washed (lysis buffer) 20uL bead volume

protein A/G beads (Millipore IP05 or Santa Cruz sc2003). Samples were immunoprecipitated for 2 hours on a nutator at 4C. Beads were washed three times with lysis buffer, once with TE and eluted twice with 150 elution buffer (20 mM Tris–HCl, pH 7.5, 5 mM EDTA, and 50 mM NaCl and freshly added 1% SDS, 50 μg/ml Proteinase K, and 20 μg/ml RNase A) for 20 minutes at 65C. Eluate was pooled and samples were reverse crosslinked overnight at 65°C. DNA fragments were extracted by addition of an equal volume of phenol:chloroform:isoamyl alcohol, ethanol precipitated and resuspended in 20ul nuclease free water. ChIP enrichment was quantified by ddPCR with EvaGreen (BioRad 1864034) on a QX100 droplet reader (Robin et al., 2014; Wylie et al., 2016). ChIP DNA values were displayed as fold enrichment over IgG. Confidence intervals were calculated as per BioRad (Wylie et al., 2016). Primer are listed in Table S6.

CUT&RUN

CUT&RUN (Skene and Henikoff, 2017) was performed using a modified version of a Drosophila specific CUT&RUN protocol (Ahmed, 2018). Approximately 100 pairs of L3 larvae salivary glands per genotype were dissected into ice cold PBS with protease inhibitors (Roche 11836170001) and immediately transferred to an eppendorf tube on ice containing 500uL of pre-chilled Wash+ buffer (20mM Hepes pH 7.9, 150mM NaCl, 0.1% BSA, 0.5mM Spermadine and protease inhibitors). Dissections were limited to 60 minutes. Dissected salivary glands were transferred to binding buffer (20MM Hepes pH 7.9, 10mM KCl, 1mM CaCl2, 1mM MnCl2) containing 15uL binding buffer equilibrated Concavalin A (BP531, Bangs Laboratories) beads and incubated for 10 minutes at room temperature. Concavalin A bound salivary glands were then placed on a magnetic rack, supernatant was aspirated and samples were resuspended and blocked for 10 minutes at room temperature in 1mL of dbe+ (Wash+ buffer supplemented with 2mM EDTA and 0.05% Digitonin). Sample was again placed on a magnetic rack, dbe+ block was aspirated and replaced with 100uL of 1:100 diluted antibody (dsRed Takara) in dbe+ buffer. Samples were gently tapped to resuspended and incubated on a nutator at 4C overnight. Samples were then spun at low speed to collect liquid, transferred to the magnetic rack and washed twice with 500uL of dbe+. Protein A MNase batch #6 (kind gift of Steven Henikoff) was diluted 1:400 into dbd+ was then added to each sample. Samples were resuspended by gently tapping and incubated 1hr at 4C on a nutator. Samples were briefly spun at low speed to collect liquid, transferred to the magnetic rack and washed twice with 500uL Wash+ buffer. Samples were then chilled on ice, resuspended in 150uL ice cold Wash+C buffer (Wash+ buffer containing 2mM CaCl2), and incubated on ice for 30 minutes. MNase reaction was stopped by the addition of 150uL 2x STOP buffer (20mM NaCl, 20mM EDTA, 4mM EGTA, 1ug RNaseA, 0.3uL 1ng/mL yeast spike-in DNA (kind gift of Steven Henikoff)) and incubation at 37C for 30 minutes. Samples were finally transferred to the magnetic rack, and supernatant containing eluted chromatin fragments was transferred to a new tube. To each supernatant tube, 2.5uL of 20mg/mL Proteinase K and 2uL of 10% SDS was added. Tubes were incubated at 50C for 2 hours. DNA fragments were purified by addition of an equal volume of phenol:chloroform:isoamyl alcohol, ethanol precipitated and resuspended in 40ul nuclease free Tris, pH 8.0. A similar protocol was utilized for all histone Cut&Run (H3K9m3 Abcam ab8898, H3K4m3 Active Motif 39159) experiments with the following modification: Protein A/G MNase (Addgene #123461) was purified as in (Meers MP, Bryson TD, Henikoff JG, Henikoff S. Improved CUT&RUN chromatin profiling tools. Elife. 2019 Jun 24;8:e46314. Doi: 10.7554/eLife.46314. PMID: 31232687; PMCID: PMC6598765.) and diluted 1:280 into dbe+ for MNase digestion step.

CUT&RUN sequencing libraries were prepared using the NEXTFLEX RAPID DNA-seq Kit 2.0 (Bioo NOVA 5188-12) following the manufacturer's protocol with modification. Briefly, the thermal cycler program for End-Repair and Adenylation was modified (30min at 20C, 75 min at 58C), adapter ligation proceeded at 8C overnight, and post-ligation NEXTFLEX bead clean-up was not size selective to retain small fragments. Pippen was used to size select libraries and remove un-ligated adapters prior to sequencing. Prepared libraries were sequenced on an Illumina NextSeq 500 (Paired End: 36bp) by the McDermott Center NGS Core at UT Southwestern Medical center.

CUT&RUN data analysis

Sequencing reads were deduplicated based on barcode using prinseq (Schmieder and Edwards, 2011) Deduplicated reads were next aligned to the yeast genome (R64-1-1) or e. coli (K12 MG1655) using bowtie2 (–local –very-sensitive-local –no-unal –no-mixed –no-discordant –phred33 -I 10 -X 700 –no-overlap –no-dovetail) to quantify levels of yeast spike-in or e. coli carryover for each sample (Langmead and Salzberg, 2012). Remaining sequencing reads were aligned with the STAR aligner (–outFilterMultimapScoreRange 2 –winAnchorMultimapNmax 1000 –alignIntronMax 1 –alignMatesGapMax 700 –outFilterMultimapNmax 10000 –outFilterMismatchNmax 5 –outReadsUnmapped Fastx –alignEndsType EndToEnd –outSAMprimaryFlag AllBestScore) to versions of the Flybase R6.18 fly genome modified to include some or all of the following, as appropriate: 1) the p53R-GFP transgene, 2) the p53R-GFP delRE transgene, 3) the mCh-p53 transgene (Dobin et al., 2013). Aligned reads were separated into nucleosome (>150bp) and subnucleosome (<120bp) resolution fragments. Spike-in yeast (Protein A samples) or carryover e. coli (Protein A/G samples) normalized bigwigs for uniquely mapped (MAPQ=255) and unique and multiply mapped reads were created using deeptools Bamcoverage (Ramírez et al., 2016).

RT-PCR

corolla, xrp1, p53 isoform and *reaper* expression was measured using digital droplet RT–PCR (RT-ddPCR) assays (Figures 6 and 7). For *corolla* expression, fly ovaries were dissected in PBS, and total RNA was isolated using TRIzol reagent (Life Technologies). Five ovary pairs per RNA preparation were used for all RT–PCR data. For *xrp1 and p53 isoform* expression in salivary glands, ~30 salivary glands per biological replicate were dissected in PBS and total RNA was isolated using TRIzol reagent (Life Technologies). For *reaper*

expression in embryos, embryos were collected for 1hr on standard juice media, aged for 3hrs, exposed to 40Gy of ionizing radiation using a Cs-137 Mark 1-68A irradiator (J.L.Shepherd & Associates, San Ferando, CA, USA) and recovered for 1.5hrs. Unirradiated controls were carried side-by-side. Embryos were dechorionated with 50% bleach, rinsed, and total RNA was isolated using TRIzol reagent. cDNA from embryos, salivary glands and ovaries was generated using iScript cDNA synthesis kit (Bio-Rad). Primers are listed in Table S6. Droplet digital RT–PCR reactions (Figures 6 and 7) were previously described (Link et al., 2013). Primers specific for the *corolla* and *reaper* transcript are listed in Table S6. *rp49* was used for normalization. All graphs were generated in Prism software and a one-way ANOVA with multiple comparisons was performed for statistical analysis. P-values are listed in Figure legends.

QUANTIFICATION AND STATISTICAL ANALYSIS

For all statistical analysis, data were placed into GraphPad Prism software and a one-way ANOVA test was performed on all genotypes, with multiple comparisons at the 95% confidence interval. Multiple comparisons were corrected for using the Tukey statistical hypothesis testing. P-values are noted in the figure legends.